

Cross section measurement methods during floods for surface velocimetry

A review of contact and non-contact methods

Prepared for Envirolink

September 2024



Prepared by:
Hamish Biggs

For any information regarding this report please contact:

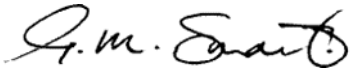
Hamish Biggs
Hydrodynamics Scientist
Hydrodynamics Group
+64 3 343 7843
Hamish.Biggs@niwa.co.nz

National Institute of Water & Atmospheric Research Ltd
PO Box 8602
Riccarton
Christchurch 8440

Phone +64 3 348 8987

NIWA CLIENT REPORT No: 2024294CH
Report date: September 2024
NIWA Project: ELF24504

Revision	Description	Date
Version 1.0	Final draft sent to client	20 September 2024
Version 1.1	Final version	7 October 2024

Quality Assurance Statement		
	Reviewed by:	Graeme Smart
	Formatting checked by:	Rachel Wright
	Approved for release by:	Phillip Jellyman

© All rights reserved. This publication may not be reproduced or copied in any form without the permission of the copyright owner(s). Such permission is only to be given in accordance with the terms of the client's contract with NIWA. This copyright extends to all forms of copying and any storage of material in any kind of information retrieval system.

Whilst NIWA has used all reasonable endeavours to ensure that the information contained in this document is accurate, NIWA does not give any express or implied warranty as to the completeness of the information contained herein, or that it will be suitable for any purpose(s) other than those specifically contemplated during the project or agreed by NIWA and the client.

Contents

- Executive summary 6**
- 1 Introduction 7**
- 2 Contact measurement methods 8**
 - 2.1 Weighted soundings 8
 - 2.2 Wading rod (small streams)..... 9
 - 2.3 Pressure transducer 10
 - 2.4 Acoustic Doppler Current Profiler (ADCP) 10
 - 2.5 Depth sounder (bridges, cableways, and boats) 11
- 3 Non-contact measurement methods 14**
 - 3.1 Ground Penetrating Radar (GPR)..... 14
 - 3.2 Depth sounder on drones (semi-contact)..... 21
 - 3.3 Depth from turbulence and surface flow characteristics 25
 - 3.4 Optical methods (not suitable during floods)..... 27
 - 3.5 Potential future method: Estimation of cross sections during floods from before and after surveys 29
- 4 Conclusions 31**
- 5 Acknowledgements 33**
- 6 Glossary of abbreviations and terms 34**
- 7 References..... 36**

- Appendix A Cross sections from moving boat ADCP gaugings..... 43**
- Appendix B Cross sections from depth sounders with GPS 48**

Figures

Figure 2-1:	Columbus type (C-type) sounding weights up to 300 lb.	8
Figure 2-2:	Depth measurements by sounding weights, corrections for downstream drift.	9
Figure 2-3:	Pressure Operated Electronic Meter (POEM) for measuring velocities and depth from bridges and cableways.	10
Figure 2-4:	Tritech PA500 depth sounder connected to Trimble R10 RTK GPS Rover and mounted on an ADCP boat hull.	12
Figure 2-5:	EchoLogger ECT D24 dual frequency echosounder (left). Echosounder deployment on an Unmanned Surface Vehicle (USV) with RTK/PPK GPS (right).	13
Figure 2-6:	Multibeam echosounder surveys of scour around bridge piers during floods.	13
Figure 3-1:	GPR measurements of flood cross section bathymetry.	14
Figure 3-2:	Helicopter deployment of GPR and doppler radar (left), comparison of GPR and reference depth measurements (centre), comparison of doppler radar and reference velocity measurements (right).	15
Figure 3-3:	Left: Deployment of a GPR antenna and doppler radar system on a cableway by Costa et al. (2006). Right: Deployment of a GPR antenna from a bridge by Hong et al. (2017).	16
Figure 3-4:	Lightweight aerial GPR antennas on DJI M600 drones.	16
Figure 3-5:	MALÅ GeoDrone80 mounted on a DJI M600 drone and deployed in the Waimakariri River, New Zealand for cross sections of bathymetry during a flood.	18
Figure 3-6:	Using nadir FPV aerial imagery from a DJI M210 drone flown by a second pilot to fine tune proximity to the far bank of the river (river width was ~300 m).	19
Figure 3-7:	Flood gauging in the Waimakariri River, New Zealand.	19
Figure 3-8:	Left: Geoscanners Gekko-80 deployed in an inflatable boat – water coupled. Centre: Radargram from water coupled antenna (clean signal). Right: Radargram from antenna in air (messy signal).	20
Figure 3-9:	Left: Tethered sonar towed by DJI M600 drone. Centre: Tethered sonar towed by DJI Phantom 4 drone. Right: Rigidly attached depth sounder on DJI M600 drone.	22
Figure 3-10:	Bathy-Drone depth sounder system, towed by a DJI M600 drone.	23
Figure 3-11:	Bathy-Drone components and forces.	23
Figure 3-12:	Left: UAWOS tethered sonar payload to measure river bathymetry. Right: SPH Engineering commercially available drone bathymetry system with the ECT D24S dual-frequency sonar.	24
Figure 3-13:	The waterproof SwellPro SplashDrone 4 (left) and setup in boat mode (right).	24
Figure 3-14:	Topo-bathymetric LiDAR, showing the RIEGL VQ-840-G.	29
Figure A-1:	Exporting bathymetry from the MAP tab of QRev. Navigation reference needs to be set to VTG for flood measurements with mobile bed sediment.	43
Figure A-2:	Data exported from QRev MAP tab as a .csv file. Duplicate rows need to be removed.	44
Figure A-3:	Using 'Distance (Left Bank) (m)' column to remove duplicate rows.	44
Figure A-4:	Data from QRev after removing duplicate rows. The 'Distance (Left bank) (m)' and 'Depth (m)' columns can now be used to generate a cross section file.	45

Figure A-5:	Cross section .csv file for use in Hydro-STIV. Extrapolation to riverbanks needs to be manually added as it is not exported from the MAP tab of QRev. Depth is also converted to negative height values.	45
Figure A-1:	Left: ADCP displacement during a transect. Right: Cross section after vector projection of North/East displacement onto cross section unit vector, and resampling (linear interpolation) of depth.	46
Figure A-2:	Left: Rescaling of linear displacement to account for drift in distance sources. Width can be manually measured and entered, or an ADCP distance source can be used (VTG in this case). Right: Multiple transects are overlain, then averaged to improve the accuracy of the result (black dashed line) and exported as a .csv file.	47
Figure B-1:	Measurement locations from are projected onto the cross section unit vector.	48
Figure B-2:	The cross section and depth measurements are linearly interpolated and smoothed.	48

Executive summary

The use of surface velocimetry methods for non-contact flood flow measurements is rapidly increasing. These methods provide a valuable tool when the use of contact measurement methods, such as Acoustic Doppler Current Profilers (ADCPs), is not possible. However, surface velocimetry methods do not directly measure cross sections (as ADCPs do) and the accuracy of calculated discharge is dependent on the use of an accurate cross section. For flood flow measurements, cross sections can change significantly due to sediment transport processes, introducing potential errors into discharge measurements if cross sections are surveyed before or after the flood, rather than cross sections being captured at the same time as surface velocities.

This report provides a literature review of contact and non-contact cross section measurement methods. It covers both traditional well-established methods and state of the art methods being developed in New Zealand and internationally.

Contact measurement methods include: Weighted soundings; Wading rods for small streams; Pressure transducers; Acoustic Doppler Current Profilers; and depth sounders deployed from bridges, cableways, and boats.

Non-contact measurement methods include: Ground Penetrating Radar; Depth sounders on drones; Depth from turbulence and surface flow characteristics; Optical methods; and potential future methods, such as interpolation between cross sections measured before and after floods.

Currently, the most suitable methods for routine deployments by council field hydrologists to measure cross sections during floods are using the Pressure Operated Electronic Meter (POEM) and acoustic methods using ADCPs or depth sounders. The development and implementation of non-contact measurement methods for bathymetry is rapidly progressing. However, many of these methods have yet to be applied to the measurement of cross sections during floods or are unsuitable during floods due to suspended sediment and low visual clarity (i.e., optical methods). The most promising non-contact methods for cross section measurements during floods are using 'depth sounders on drones' and 'ground penetrating radar'. However, both methods still require scientific and technical development, before they are suitable for routine operations.

1 Introduction

Floods are increasing in magnitude and frequency in New Zealand due to climate change. Flood flow measurements are essential for developing stage-discharge rating curves, providing public safety warnings, developing hazard maps, allocating water resources (i.e., flood harvesting), quantifying fine sediment transport, evaluating flushing flows, and assessing the long term state and trends of river flows (i.e., the effects of climate change). Reliable information on flood magnitudes and their trends is also necessary to design flood protection measures (such as stop banks), assess infrastructure risks, and determine land zoning (such as flood hazard areas).

Measurement of large floods poses an ongoing challenge for councils around New Zealand and deployment of instream equipment is not possible in many cases. There are also serious safety risks to council staff if they are attempting to perform instream measurements during large floods. To address these issues flow measurement techniques based on surface velocimetry have been deployed by many councils around New Zealand. These techniques enable non-contact discharge gauging, which improves staff safety, and enables the measurement of large floods that were not previously possible. Surface velocimetry methods commonly in use are doppler radar from bridges and cableways (e.g., Welber et al. 2016), surface image velocimetry from riverbanks (oblique imagery) (e.g., Le Coz et al. 2010), and surface image velocimetry from drones (e.g., Randall 2021). Surface image velocimetry videos are typically processed using either Space-Time Image Velocimetry (STIV) (Fujita et al. 2019), or Large Scale Particle Image Velocimetry (LSPIV) (Muste et al. 2008). Commonly used software packages for processing data are Hydro-STIV (Hydro Technology Institute, 2022), Fudaa-LSPIV (Jodeau et al. 2019), RIVeR (Patalano et al. 2017), and TRiVIA (Legleiter and Kinzel 2023).

Surface velocimetry methods require a river cross section (depth profile), to calculate discharge. Occasionally measurements can be carried out where the cross section is immobile (concrete lined channels, or bedrock reaches), but even these reaches may have sediment flowing across the bed, affecting the depth. Cross sections are typically measured before/after a large flood where surface velocimetry methods are required; however, cross sections can change substantially during floods (McMillan et al. 2010; Williams et al. 2015), with significant impacts to flood hydraulics (Guan et al. 2016; Rickenmann et al. 2016; Wyżga et al. 2016), and discharge accuracy (McMillan et al. 2010). Riverbed substrate and 'bed roughness' can also change during floods, with further impacts to flow hydraulics (Ferguson 2007; Yadav et al. 2022) and thus discharge accuracy from surface velocimetry. There is currently little known in the international literature about how cross section changes during floods impact discharge estimates made with surface velocimetry methods, and how uncertainties should be quantified. To minimise uncertainties in discharge estimates, cross sections should be measured at the same time as surface velocities; however, this can be technically challenging, and is an active area of research in New Zealand and internationally.

This report provides a review of methods for measuring cross sections during floods. It covers both contact (Section 2) and non-contact methods (Section 3), with coverage of existing established methods, as well as cutting edge methods being developed in New Zealand and internationally.

2 Contact measurement methods

2.1 Weighted soundings

Flood cross sections are commonly measured from bridges, cableways, or boats, using sounding reels (gauging reels) and sounding weights (Rantz 1982; Turnipseed and Sauer 2010; NEMS 2013). Sounding weights are typically streamlined and heavy (Figure 2-1), to reduce drag forces and downstream drift which results in sounding lines that are not vertical (Figure 2-2). Corrections to the downstream drift of sounding weights can be made following Turnipseed and Sauer (2010) or ISO748 (2007).

If velocities are excessive and/or depths are deep, the sounding weight may not be able to reach the bottom, the downstream drift may render the angle too great for accurate measurement, or the bed may not be able to be detected or 'felt' by the operator.

If the sounding weight has an integrated pressure transducer (see Section 2.3) it is possible to measure depth without knowing distances to the water surface, or correcting for sounding line downstream drift. When using sounding weights care must be taken around debris moving down the channel, notably trees/logs. It is prudent to have an upstream observer and a quick release, or designed failure point (i.e., shear pin on the hanger bar) if the sounding weight and sounding line become tangled (Turnipseed and Sauer 2010).

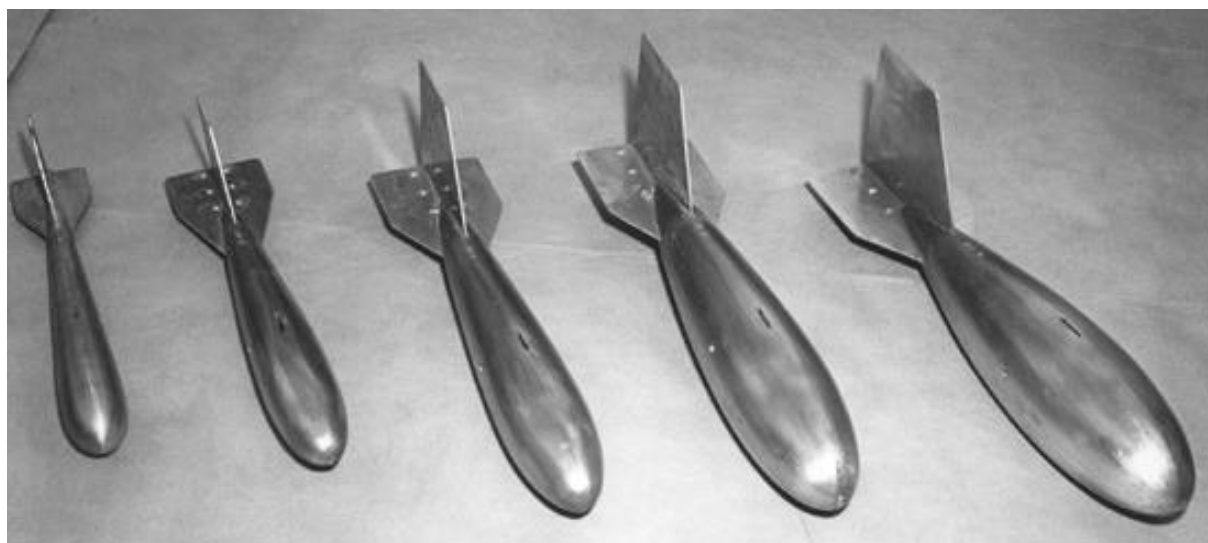


Figure 2-1: Columbus type (C-type) sounding weights up to 300 lb. Image from www.prph2o.com.

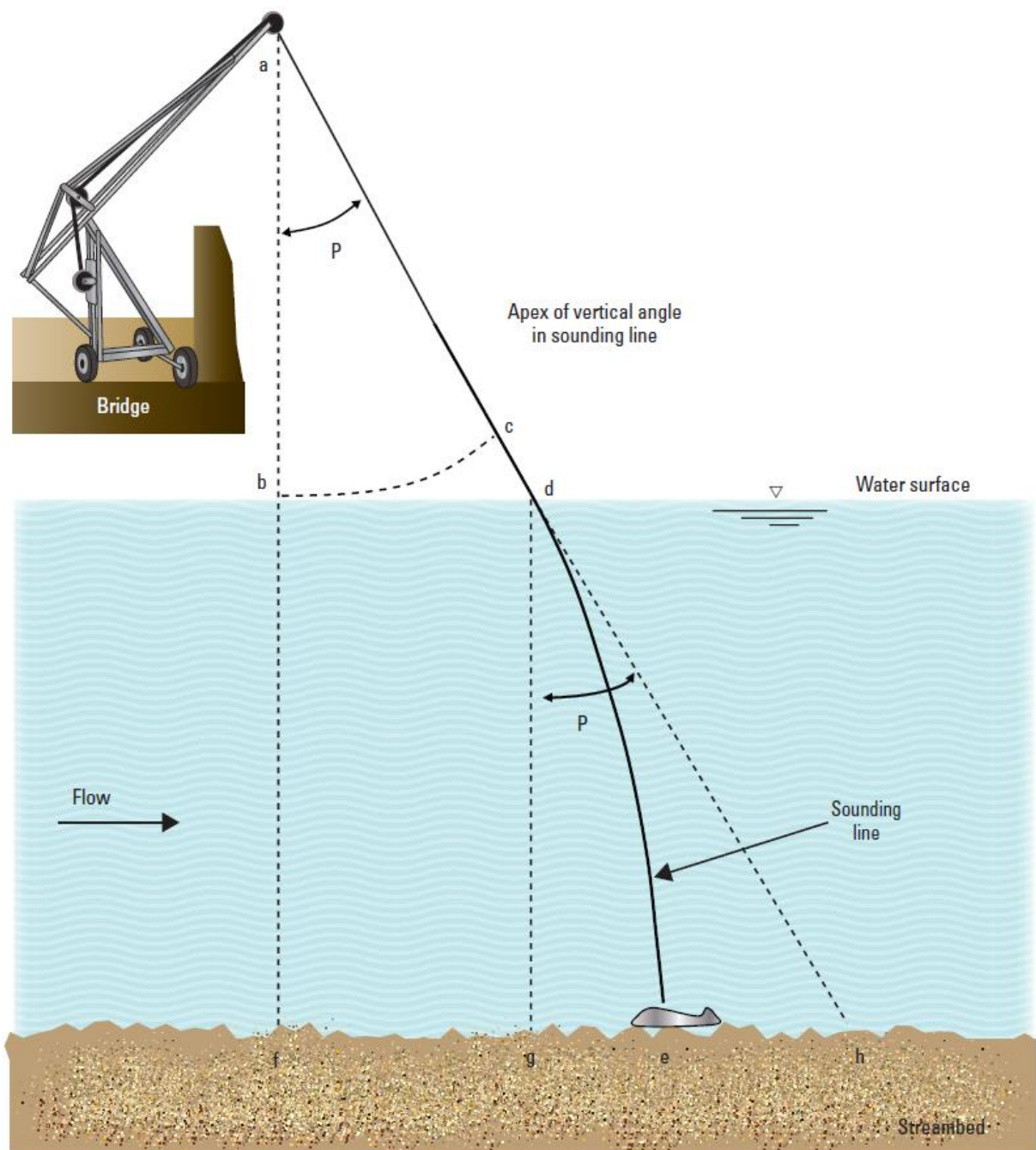


Figure 2-2: Depth measurements by sounding weights, corrections for downstream drift. Image from Turnipseed and Sauer (2010).

2.2 Wading rod (small streams)

In small streams it may be possible to use a wading rod to measure cross sections during floods. Although this will be highly dependent on the depth, slope, and water velocity of the stream to achieve instream measurements safely. It may also be possible to use wading rods, survey staffs, or similar to measure cross sections of small streams from bridges during floods.

2.3 Pressure transducer

Similar to sounding weights the Pressure Operated Electronic Meter (POEM) can be used for measuring depths and cross sections during floods (Smart 1991; Nikora and Smart 1997; NEMS 2013). It has a water inlet at the front for measuring dynamic pressure (velocity head) and also water inlets at the side for measuring static pressure (water depth). The POEM can be deployed from bridges, cableways, and boats, but does not need cable length to be measured, or corrections made for downstream drift. This provides a significant advantage over sounding weights for measuring depth, and coupled with its measurements of velocity, provides a complete solution for flood flow gauging from bridges, cableways, and boats. When deploying the POEM, air pressure at the water surface should first be recorded by the instrument, so that accurate depths can be calculated from hydrostatic pressure.



Figure 2-3: Pressure Operated Electronic Meter (POEM) for measuring velocities and depth from bridges and cableways.

2.4 Acoustic Doppler Current Profiler (ADCP)

ADCPs provide a convenient way to measure cross section bathymetry; however, their operations during floods can be limited by instream debris, river velocities, and near bed suspended sediment. In large floods the depth sounder on an ADCP may not be able to identify the riverbed, and the use of a lower frequency (or dual frequency) depth sounder may be needed (Section 2.5). If an ADCP can be used during a flood to obtain bathymetry, then it can usually also collect reliable velocity data, making the use of surface velocimetry methods unnecessary. If an ADCP is able to collect reliable depth data, but not reliable velocity data during a flood, then it can still be used for measuring cross sections during floods, with the methods for extracting cross section data described below.

ADCP Bathymetry – Section-by-Section (SxS Pro)

Bathymetric cross sections can be easily obtained from ADCPs by doing a section-by-section gauging. For Teledyne RDI ADCPs this is performed in the software SxS Pro. With this approach the ADCP is manually positioned at regular intervals across the cross section (e.g., 20–30 verticals). The ADCP records a velocity profile and depth at each location, from which mean velocities and discharge are computed. This is a common method for ADCP flood gauging when there are mobile bed conditions. This is also a very convenient way to obtain a cross section for use with surface velocity measurements, as it is provided in the output gauging summary file. The main downside is that the ADCP displacement is manually reference to the bank, which can introduce minor errors due to any stretch or sag in tape

measures/tag lines (if not accounted for), or downstream drift of the ADCP from a perpendicular cross section line. Alternative ways to measure displacement from the bank (such as with a laser range finder) can help to avoid/reduce these uncertainties.

ADCP Bathymetry – Moving boat

Bathymetry data from ADCPs can also be extracted from moving boat data. During floods the riverbed will typically be mobile, so GPS (GGA or VTG) will be needed for positioning data, since Bottom Track (BT) will not provide an accurate position. Typically, VTG is used in New Zealand, since differential GPS corrections with SBAS (Satellite Based Augmentation System) are not yet available¹ and are needed for accurate positioning using GGA. It is also possible to use a Real Time Kinematic Global Positioning System (RTK GPS) or Post Processed Kinematic GPS (PPK GPS); however, this is beyond what can be expected for routine deployments.

Raw ADCP position and depth data can be exported from WinRiver II (Teledyne RDI ADCPs) and RiverSurveyor Live (Sontek ADCPs); however, this can be cumbersome and has some fundamental limitations:

- ADCP paths are not straight and must be accounted for, including loops.
- There are multiple distance references available (i.e., GGA, VTG, BT), with drift in displacement estimates between the references.
- Riverbanks must be accounted for.
- Cross section direction must be accounted for.
- Preprocessing data for QA/QC is usually needed (e.g., removing bad transects).

To account for these issues, it is better to pre-process data in QRev² (or QRevInt³) then export bathymetry from the 'MAP' tab and manipulate it in excel to generate cross section files.

Alternatively, QRev .mat files can be processed using a tool from the 'drone flow' software toolbox (Biggs 2022) to generate cross section files.

Further information on applying these methods is provided in Appendix A.

2.5 Depth sounder (bridges, cableways, and boats)

When measuring cross sections during large floods, high suspended sediment concentration near the riverbed may limit the ability of ADCP depth sounders to distinguish the bottom of the channel. In this case lower frequency, dual frequency, or higher power depth sounders may be needed. Depth sounders (echosounders) can be deployed from bridges, cableways, manned boats, remote control boats, or on ADCP boat hulls.

ADCPs and depth sounders are also susceptible to air entrainment across the face of the depth sounder at high velocities, which can interfere with acoustic measurements. It is important to deploy depth

¹ It is currently being developed and will be known as SouthPAN (Southern Positioning Augmentation Network)

<https://www.lin.govt.nz/data/geodetic-services/satellite-based-augmentation-system>

² <https://hydroacoustics.usgs.gov/movingboat/QRev.shtml#Download>

³ <https://www.genesishydrotech.com/qrevint>

sounders in a suitably shaped streamlined shroud/enclosure/hull, to minimise the entrainment of air at high velocities during floods.

Suitable depth sounders require an internal Inertial Measurement Unit (IMU) or device capable of measuring depth sounder inclination, to correct for pitch and roll during measurements. A means of determining the depth sounder position is also needed (i.e., measurement origin). This can be achieved simply by referencing cross stream position to a fixed point on the channel bank, then using a tagline (or tape measure), or laser rangefinder to measure cross stream displacement. Alternatively, position data can be logged with RTK GPS or PPK GPS, which provides highly accurate (i.e., 1–3 cm) data on the location of the depth sounder (Figure 2-4).



Figure 2-4: Tritech PA500 depth sounder connected to Trimble R10 RTK GPS Rover and mounted on an ADCP boat hull.

Dual frequency narrow beam echosounders

There are a wide range of echosounders available on the market; however, one model of note is the Echologger EU D24 (USB interface) or ECT D24 (RS-232 or RS-485 interface)⁴. This echosounder is very compact (56 mm diameter × 80 mm length) and light weight (240 g without cable). It features transmissions at both 200 kHz (10° conical beam) and 450 kHz (5° conical beam), with an internal tilt sensor, and has an adjustable transmission power up to 50 W (Figure 2-5: Left). It can be easily integrated with GPS and is well suited for a wide range of bathymetric surveying applications, from cross sections during floods, to assessment of scour around bridge piers, or surveys in vegetated channels, where lower frequency transmissions can help to penetrate aquatic vegetation to delineate the channel bed. It can be deployed on Unmanned Surface Vehicles (USVs) (Figure 2-5: Right), manned boats, or even drones (see Section 3.2). For tethered deployment from bridges or cableways it may need to be integrated into a surface float to maintain approximately vertical orientation and consistent submergence depth.

⁴ <https://www.echologger.com/products/dual-frequency-echosounder-shallow>



Figure 2-5: EchoLogger ECT D24 dual frequency echosounder (left). Echosounder deployment on an Unmanned Surface Vehicle (USV) with RTK/PPK GPS (right). Images from <https://www.echologger.com/>.

Multibeam echosounders

Multibeam echosounders collect a swath of bathymetry data and can be used for larger scale mapping, such as measurements upstream and downstream of a cross section to assess scour around bridge piers (Dietsch et al. 2014). However, these systems are typically much larger and more expensive than single beam echosounders and are not needed for flood gauging where only a 2D cross section is required.

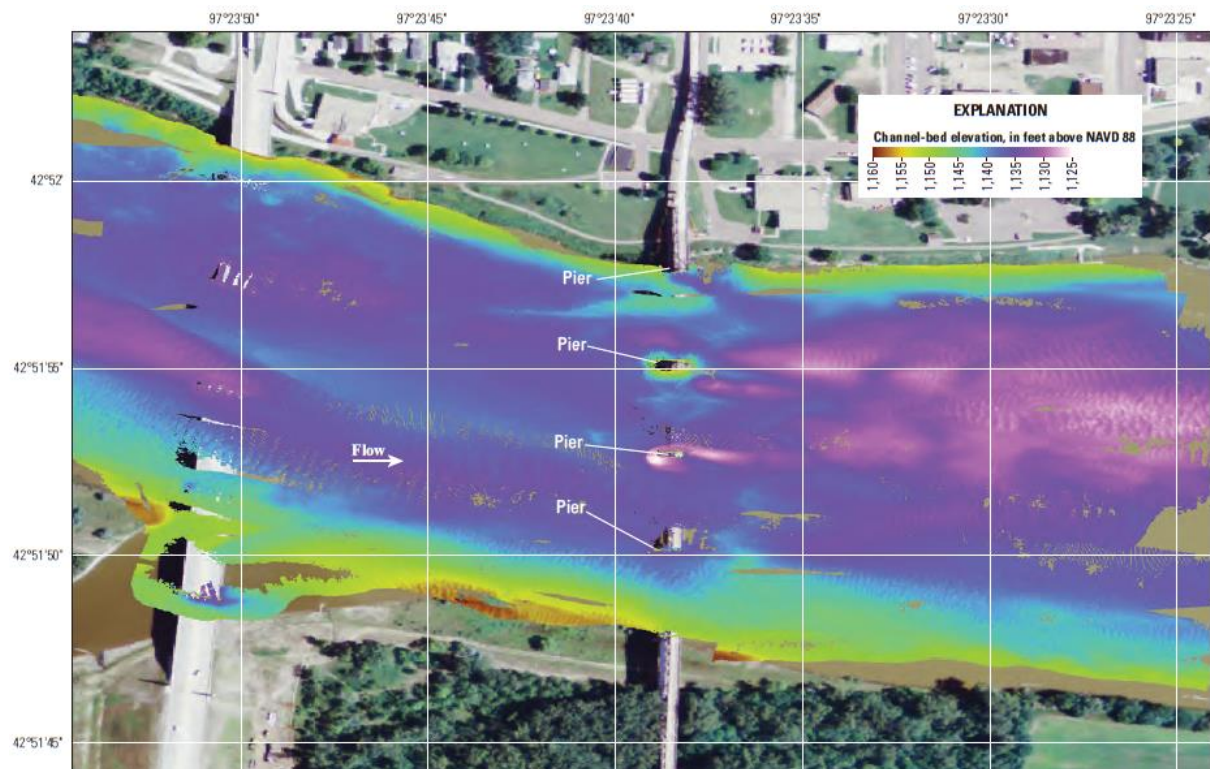


Figure 2-6: Multibeam echosounder surveys of scour around bridge piers during floods. Image from Dietsch et al. (2014).

3 Non-contact measurement methods

3.1 Ground Penetrating Radar (GPR)

GPR - Historical applications

GPR has been used to measure bathymetry since the 1970s, with initial work focusing on towed GPR systems over frozen water bodies to measure ice thickness and water depth under the ice (Annan and Davis 1977). The use of GPR for measuring cross section bathymetry during floods was first demonstrated by Spicer et al. (1997), using a 100 MHz antenna suspended from a cableway. They reported that channel cross sectional area was estimated within $\pm 20\%$ or better compared to weighted soundings, with areas close to channel banks contributing to lower accuracy. They predicted that accuracy of $\pm 10\%$ could be achieved with better calibration of signal velocity to local conditions. They found that GPR provided advantages over weighted soundings, since it produced continuous cross sections rather than point measurements and could be acquired quickly. From repeated cross section surveys Spicer et al. (1997) also found significant bed movement and changes in cross sections as gravel bedforms passed under the cableway. This illustrates the importance of cross section measurements that are concurrent with velocity measurements during bedload transport when cross sections are changing.

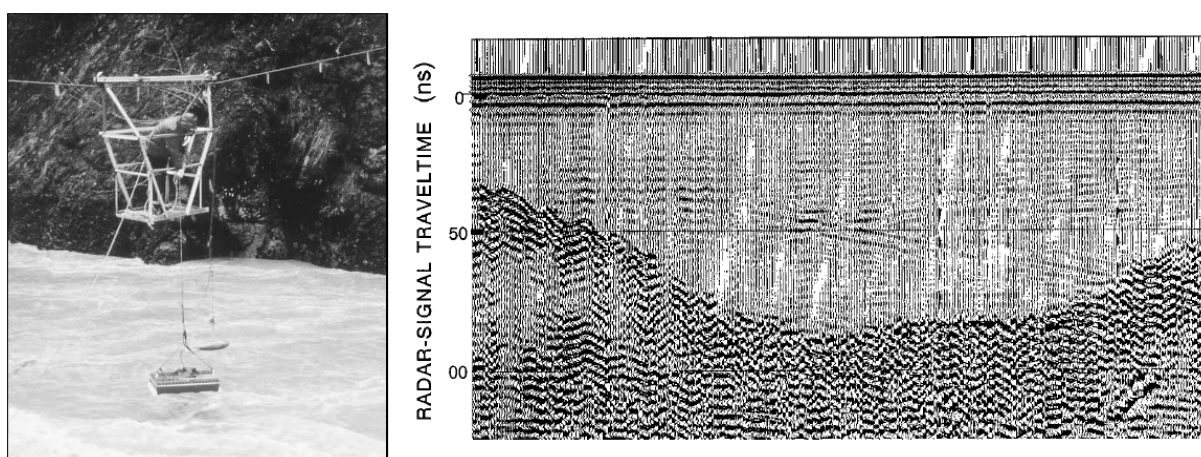


Figure 3-1: GPR measurements of flood cross section bathymetry. Images from Spicer et al. (1997).

Further progress was made by Costa et al. (2000) with a GPR antenna again deployed from a cableway and suspended above a river, but with surface velocities measured using a pulsed doppler radar operating at a frequency of 10 GHz. This enabled non-contact measurements of both the cross section and surface velocities, from which discharge was calculated. Results closely matched reference discharge measurements with an ADCP and the well-established rating curve at the test site, with mean ADCP discharge of $520 \text{ m}^3/\text{s}$ and mean radar discharge of $518 \text{ m}^3/\text{s}$ (see Table 1 of Costa et al. 2000), demonstrating the feasibility of the method.

The first aerial discharge gauging using GPR and doppler radar was performed by Melcher et al. (2002) with a 100 MHz MALÅ GeoScience GPR antenna and a 10 GHz pulsed doppler radar deployed on a Bell 206B Jet Ranger helicopter (Figure 3-2: Left). Helicopter origin was recorded using Differential GPS (DGPS) and helicopter orientation was recorded using an Attitude and Heading Reference System (AHRS), similar to an Inertial Measurement Unit (IMU). These data were then used to spatially reference GPR bathymetry and doppler radar surface velocity measurements. Reference depth

measurements were made using sounding weights and an ADCP (Figure 3-2: Centre). Reference velocity measurements were made using a Price AA current meter and an ADCP (Figure 3-2: Right). There was good correspondence between depth and velocity measurements from radar and conventional methods, resulting in measured discharge of 226 m³/s for the reference measurement, compared to 223 m³/s from radar. While it must be acknowledged that the use of helicopters for measuring river and flood discharge is not necessarily cost effective, nor particularly safe, this work provided a pioneering proof of concept for aerial remote sensing of river flow.

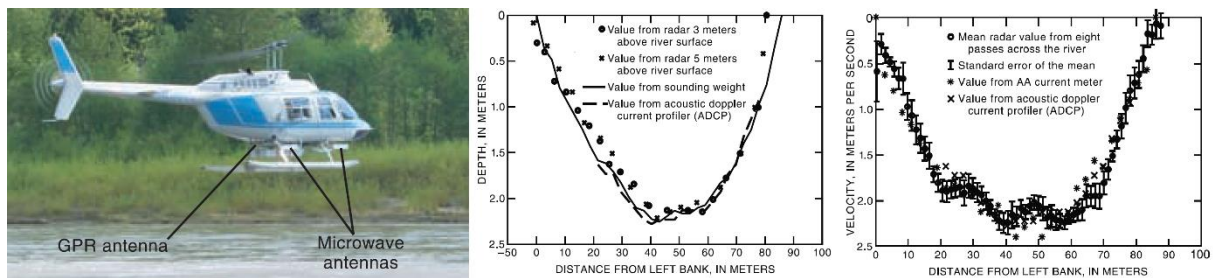


Figure 3-2: Helicopter deployment of GPR and doppler radar (left), comparison of GPR and reference depth measurements (centre), comparison of doppler radar and reference velocity measurements (right). Images from Melcher et al. (2002).

Flood discharge gauging using a GPR antenna and doppler radar suspended from a cableway (Figure 3-3: Left) was also performed by Costa et al. (2006). The measurement system was comprised of a 100 MHz MALÅ GeoScience Ramac X3M Corder GPR antenna and a 24 GHz doppler radar (RiverScat), developed by the University of Washington. The team gauged a flood of 1,054 m³/s, compared to a reference discharge of 1,039 m³/s.

Flood discharge gauging using GPR was also undertaken by Hong et al. (2017), with the GPR antenna deployed from a bridge (Figure 3-3: Right) to measure cross sections during typhoons and during the monsoon period in Taiwan. However, their methodology was more primitive than that of Costa et al. (2006) as they only deployed a Surface Velocity Radar (SVR) system (i.e., doppler radar) at a single fixed location on the bridge, rather than moving it across the river to provide a distribution of surface velocities to couple with the cross section from GPR for discharge estimation.



Figure 3-3: Left: Deployment of a GPR antenna and doppler radar system on a cableway by Costa et al. (2006). Right: Deployment of a GPR antenna from a bridge by Hong et al. (2017).

GPR on drones

The rise of drones for remote sensing has been matched by the development of lightweight GPR antennas and data collection electronics (Lane et al. 2020; Dawson et al. 2021). This enables GPR cross sections to be measured at locations without a cableway or bridge (Costa et al. 2000), and without requiring expensive helicopter deployments (Melcher et al. 2002). The development of routine (and accurate) methods for evaluating surface velocities from the air, such as LSPIV and STIV using aerial imagery has enabled completely non-contact flood gauging, with drone borne GPR used for cross section measurements (Biggs 2022). There are now a range of lightweight GPR antennas available, such as the MALÅ GeoDrone80 (Figure 3-4: Left), Geoscanners Gekko-80 (Figure 3-4: Centre), and RadarTeam Cobra SE-150 (Figure 3-4: Right).

The follow sections provide an example of using a drone borne GPR to perform flood gauging in New Zealand. However, there are still significant limitations preventing the widespread adoption of GPR for cross section measurement, with these issues discussed at the end of this section.



Figure 3-4: Lightweight aerial GPR antennas on DJI M600 drones. Left: MALÅ GeoDrone80 (Biggs 2022). Centre: Geoscanners Gekko-80 (Bandini et al. 2023). Right: RadarTeam Cobra SE-150 (Image from: <https://shop.sphengineering.com/products/cobra-plug-in-gpr>).

GPR on drones – Flood measurement example New Zealand

The aerial GPR system we tested was a MALÅ GeoDrone80 (Figure 3-5: Left). It has a weight of 3.23 kg (including batteries) with a centre frequency of 80 MHz. It has two antennas (one for transmit and one for receive), a central acquisition and processing unit, and a GNSS antenna cable. It can be easily mounted on a DJI M600 drone, with an additional GNSS antenna added to the top of the drone for GPS. The MALÅ GeoDrone80 was deployed to measure a flood in the Waimakariri River (Figure 3-5).

Cross sections were initiated with the GeoDrone80 handheld unit, then stored locally on the GPR antenna during the measurement and downloaded to the handheld unit after the cross section was completed. Due to poor Wi-Fi range and interference, the GPR cross sections needed to be commenced at takeoff, then downloaded when the GPR antenna returned, with measurements split into cross section passes during post processing in the software GPR Slice. GPR systems can be flown manually, or with automatic flight paths. However, automatic flight paths are risky due to the very low recommended flight altitude of the GPR unit (~2–5 m). Any deviations in measured altitude from barometric pressure by the drone could result in a crash if not observed and corrected for manually. It is also risky to deploy the aerial GPR system at sites with riparian vegetation (i.e., some braided rivers), or to obtain cross sections up to the far bank of the river, where collision with overhanging riparian vegetation can occur. As such, we flew the MALÅ GeoDrone80 manually during all field tests, paying close attention to reported altitude, observed altitude, and proximity to obstacles. It is very hard to judge horizontal distance/displacement from ground level, and we used a second spotter drone hovering over the far bank with its camera pointing nadir to enable the GPR unit to be flown within a safe distance of the far bank and overhanging riparian vegetation (Figure 3-6).

GPR data were pre-processed in the software GPR Slice⁵, to trim GPR data to a single transect (cross section), define the water surface elevation, define the bed elevation, and thus extract depth. This data was then exported as a text file with fields 'Easting_m', 'Northing_m', and 'Depth_m', in the NZTM2000 coordinate system. The locations of the banks were manually added to the file as the first and last data records, with zero depth. Data were then imported into MATLAB where they were processed with the script 'processGPCrossSection.m' to project, resample, and interpolate data to obtain the cross section (Biggs 2022).

Surface velocimetry videos were recorded with a DJI M210 drone, then processed in the software HydroSTIV to obtain surface velocities, with the GPR cross section used in that software to obtain discharge (Figure 3-7). The calculated discharge⁶ was 749.7 m³/s, which compares to a rated discharge at the site from ECAN of 813.7 m³/s. There were no reference discharge or cross section measurements available. The discrepancy of -7.9% may have arisen from depth errors from GPR (i.e., too shallow), selection of an alpha value that was too low⁶, surface velocities errors (i.e., too low), or errors in the rated discharge (less likely if the rating is well maintained and regularly updated). Most likely it was a cumulative combination of factors.

Although this was a useful proof of concept, it was hard to distinguish the water-bed interface in radargrams near the banks. This was attributed to interference from “through air reflections” off other interfaces. Through air reflections are due to the signal not being transmitted only vertically below the drone, but the radiation pattern being broader, with the signal travelling more quickly through air than through water, such that interfaces/objects from relatively far away (such as objects on riverbanks)

⁵ Data processing in GPR Slice was performed by John-Mark Woolley. Different GPR propagation velocities need to be applied for through air and through water transmissions. User best judgement was applied to define reflections off the riverbed.

⁶ Discharge was calculated using a surface velocity to depth averaged velocity ratio (i.e., alpha) of 0.9. This value was used because the river was more than 2 m deep and there were no velocity profiles or further information from which α could be estimated (Biggs et al. 2023).

are detected in radargrams. There were also issues with the MALÅ GeoDrone80 recording and downloading data, with system faults on subsequent missions. The data recorded by the MALÅ GeoDrone80 were very messy (likely unshielded dipole antennas) and there may be better aerial GPR antennas that produce cleaner bathymetric measurements, such as the semi-shielded Cobra SE-150 antenna from RadarTeam (Figure 3-4: Right) that is designed to be air-coupled.

Water coupled deployment of GPR antennas to improve accuracy is discussed subsequently, along with other limitations of GPR, potential solutions, and regulatory considerations.



Figure 3-5: MALÅ GeoDrone80 mounted on a DJI M600 drone and deployed in the Waimakariri River, New Zealand for cross sections of bathymetry during a flood. Image from Biggs (2022).



Figure 3-6: Using nadir FPV aerial imagery from a DJI M210 drone flown by a second pilot to fine tune proximity to the far bank of the river (river width was ~300 m). Image from Biggs (2022).

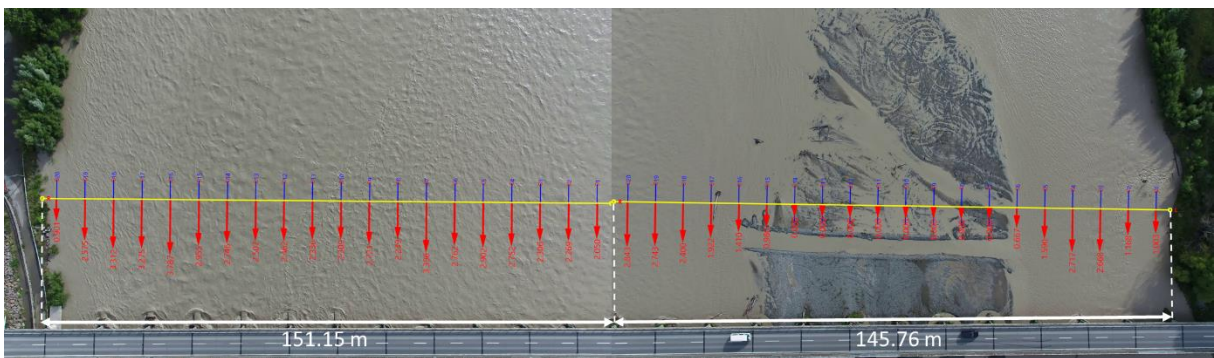


Figure 3-7: Flood gauging in the Waimakariri River, New Zealand. Image from Biggs (2022).

GPR water coupled vs through air

The deployment of GPR systems and data processing are non-trivial and require specialist expertise. Significant post processing of data is required, as well as interpretation of the water-bed interface. The deployment of drones in air results in signals that not very clean, due to reflections from other interfaces not directly underneath the antenna, as well as having less penetration power into the water, making the riverbed harder to distinguish. Better results are achieved with a water coupled antenna, where the GPR antenna is deployed in an inflatable boat (Figure 3-8: Left), since the bottom of the boat does not interfere with the GPR signal (as would occur with a metal bottom boat). This results in much cleaner radargrams (Figure 3-8: Centre), compared to deployment in air above the water surface (Figure 3-8: Right). However, this somewhat defeats the purpose of using GPR antennas for measuring cross sections during floods, since if it is possible to deploy an inflatable boat from a bridge or cableway, then a depth sounder could be used for depth measurements.

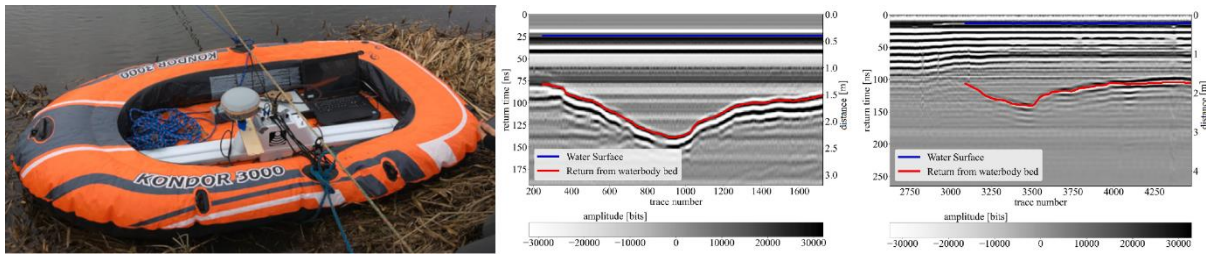


Figure 3-8: Left: Geoscanners Gekko-80 deployed in an inflatable boat – water coupled. Centre: Radargram from water coupled antenna (clean signal). Right: Radargram from antenna in air (messy signal). All images from Bandini et al. (2023).

GPR on drones – Current limitations and issues

Aerial GPR has exciting prospects, yet there are major scientific hurdles to overcome. Most aerial GPR antennas do not transmit the signal only vertically beneath the drone, but the radiation pattern is broader. Since the dielectric constant (i.e., relative dielectric permittivity) of air is much lower than that of water (Annan 2003; Baker et al. 2007) through air GPR transmissions can pick up reflections from interfaces that are relatively far away, and mask (or add noise) to the detection of the water-sediment interface (i.e., riverbed). This is particularly problematic for aerial GPR cross sections near riverbanks (Biggs 2022). To address this issue new methods are needed to reduce or filter out through air reflections to reduce noise in aerial GPR data and accurately measure water depths up to riverbanks. Potential solutions include: (1) Crossed dipoles (i.e., transmit and receive antennas at 90 degree orientation), which would require scattering at the water sediment interface (polarisation change); (2) Rotating drone and antennas during flight. Interfaces directly below the drone (or horizontal planes) will remain at the same signal time/depth, whereas other reflections will be transient; (3) Ray tracing algorithms to filter out strong reflections from terrestrial objects/interfaces (i.e., riverbanks). Alternatively, there may be antennas with better directionality and better coupling with the air such as the RadarTeam Cobra SE-150 (Figure 3-4: Right) that can provide cleaner data near channel banks.

Other issues limiting the deployment of aerial GPR systems for flood cross section measurement are:

- Cost of GPR systems, drones, and data processing software.
- Specialise expertise for deployment and processing.
- Low flight altitude making missions risky.
- An additional drone and pilot may be needed for assessing proximity to far channel banks. Alternatively, a FPV camera could be installed on the drone-borne GPR system.
- Riparian vegetation on channel banks, limiting the collection of bank-to-bank cross sections in some cases.
- Minimum water depths, with 0.3-0.4 m for water coupled GPR compared to 0.8–1.1 m for drone-borne GPR reported by Bandini et al. (2023).
- Potential regulatory issues if drone-borne GPR systems are causing interference (see below).
- Flying in the rain (i.e., waterproofing of GPR antennas, data loggers, receivers/controllers, and using a waterproof drone).

Potential regulatory issues

GPR systems suitable for flood cross section measurement radiate in the VHF band between 30 MHz and 300 MHz. The use of ground probing/penetrating radar is permitted in New Zealand⁷; however, most systems are typically ground coupled with negligible transmissions into the air. Although the MALÅ GeoDrone 80 is sold in New Zealand⁸ it is not clear from technical specifications or documentation what the transmission power and directionality is and whether it poses an interference risk. While most deployment of drone-borne GPR systems for flood flow measurement will be at remote locations, care should be taken than deployments are at very low altitudes and interference does not occur to other radio spectrum users. This is most notable in urban areas, or near sensitive infrastructure and facilities, such as airports. Further clarification that the GPR systems conform to regulations in New Zealand^{7,9}, and advice on their deployment is needed before widespread adoption. It would also be prudent to assess shielding effectiveness between GPR antenna models (Figure 3-4) and determine whether additional shielding is needed to block any transmissions not directed into the water/ground below the drone.

Additional applications

GPR could also be used for assessing sediments under riverbeds, which may be useful for estimating erosion risks and cross section changes during floods.

GPR could also be deployed in a stationary position to measure bedform migration during floods.

Summary

While the deployment of GPR for cross section measurement during floods shows clear promise, further research is needed before it becomes a viable method for widespread adoption by councils around New Zealand. There may also be other methods, such as depth sounders on drones (see next section) that provide similar (or better) measurements of cross sections, but at a lower cost, with less specialist expertise, without RF interference risks, and with easier data collection/processing.

3.2 Depth sounder on drones (semi-contact)

The deployment of light weight depth sounders from drones provides a promising method for measuring cross sections during floods. This would enable cross section measurements in locations without a cableway or upstream bridge from which a tethered boat (see Section 2.5) could be deployed. It also provides significant safety benefits compared to deployment of manned boats during floods. The use of lightweight depth sounders also means that they can be lifted out of the water if debris (i.e., trees) are approaching from upstream.

Pioneering work with drone deployed sonar was achieved by Bandini et al. (2018) using the Deeper Smart Sensor PRO+ sonar system (Figure 3-9:Left). This sonar is a single-beam echo sounder with two frequencies: 290 and 90 kHz, with 15° and 55° beam angles, respectively. Similar models of this sonar have also been towed by a DJI Phantom 4 drone (Figure 3-9: Centre) by Koutalakis and Zaimis (2022) and rigidly attached to a DJI M600 drone (Figure 3-9: Right) by Coppo Frias et al. (2024).

The work of Koutalakis and Zaimis (2022) was notable as they also measured surface velocities from the air, then coupled them with bathymetry from the towed sonar system to estimate discharge.

⁷ <https://www.rsm.govt.nz/licensing/frequencies-for-anyone/ground-and-wall-probing-radar-gurl>

⁸ <https://gprsolutions.co.nz/mala-geo-drone-80/>

⁹ <https://gazette.govt.nz/notice/id/2015-go6667?year=2015¬iceNumber=6667>



Figure 3-9: Left: Tethered sonar towed by DJI M600 drone. Centre: Tethered sonar towed by DJI Phantom 4 drone. Right: Rigidly attached depth sounder on DJI M600 drone. Image credits (left to right) are: Bandini et al. (2018), Koutalakis and Zaimis (2022), Coppo Frias et al. (2024).

Further progress was made by Diaz et al. (2022) with the development of the Bathy-Drone system (Figure 3-10). It uses a Lowrance Elite ti7 recreational fish-finder and a skiff-like planning hull, with trim plate and fins (Figure 3-11). Future iterations of the design will include RTK/PPK GPS and an IMU in the towed sonar system, making it stand alone so that it can be towed by any drone with sufficient payload capacity.

V-hull and trimaran hulls were also considered by Diaz et al. (2022) in addition to the skiff-like planning hull that was used. However, for their application of mapping inland water bodies (i.e., lakes, ponds etc), with a grid of measurements, they found that v-hull and trimaran hulls were unstable during turns. The skiff-like planning hull tracked level through the speed range of 0–24 km/h making it well suited for the high surface velocities during flood gauging; however, for flood gauging applications a survey grid that necessitates sharp turns at the end of survey lines is not needed and other hull types (i.e., longer V-Hull) may track better through flood waters and cut through surface waves reducing the downstream force. It may also get the sounder deeper in the water without air entrainment. For measurement of flood cross sections with high suspended sediment near the bed alternative narrow beam dual frequency echosounders may also perform better than the Lowrance Elite ti7, which is better suited for bathymetric surveys of lakes and ponds that require broader coverage.



Figure 3-10: Bathy-Drone depth sounder system, towed by a DJI M600 drone. Image from Diaz et al. (2022).



Figure 3-11: Bathy-Drone components and forces. Image from Diaz et al. (2022).

Measurements of river bathymetry using an EchoLogger ECT series echosounder have been completed by the Unmanned Airborne Water Observing System (UAWOS) project team (Figure 3-12: Left). With the system commercially available from SPH Engineering (Figure 3-12: Right). The echosounder features inbuilt tilt correction; however, spatial positioning relies on GPS measurements from the drone, and corrections for tether length and angle. It is unclear how well this system would perform in flooded rivers with high surface velocity and whether the echosounder would maintain an approximately vertical orientation.

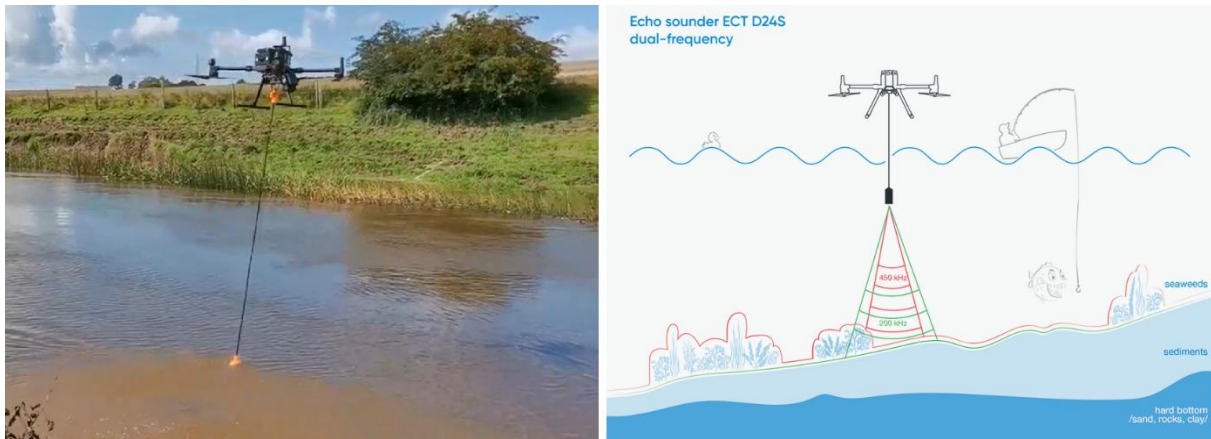


Figure 3-12: Left: UAWOS tethered sonar payload to measure river bathymetry. Right: SPH Engineering commercially available drone bathymetry system with the ECT D24S dual-frequency sonar. Image credits, Left: <https://uawos.dtu.dk/payloads/tethered-sonar>, Right: <https://shop.sphengineering.com/products/el-ect-d24s>.

Drone echosounders for flood cross sections - Future work

Previous work with drone echosounders has focused on mapping inland water bodies (i.e., lakes and ponds), or slowly flowing rivers. To our knowledge there have been no deployments for flood gauging to date. There remains a distinct knowledge gap to develop a system suitable for flood gauging with high surface velocities and harsh weather conditions (i.e., rain and wind). The design of such a system could be based around a planning hull similar to that developed by Diaz et al. (2022); however, a catamaran or trimaran hull may be more stable and track better for deployment in flooded rivers with high surface velocities and waves. A lightweight dual frequency echosounder such as the EchoLogger ECT D24 could then be incorporated into the boat hull, along with a light weight RTK/PPK GPS system such as the Emlid Reach M2.

The developed system should be stand-alone (i.e., not relying on the drone for GPS measurements), and light weight (i.e., low towing resistance). Enabling it to be deployed by any robust waterproof (or water resistant) drone, such as the SwellPro SplashDrone 4 (max payload of 2kg) or DJI Matrice 300 (max payload of 2.7 kg). Larger water-resistant drones such as the Aeronavics Skyjib (max payload of 7 kg) could also be used; however, for a cost effective and easy to use system the payload should be suitable for deployment by consumer drones such as the SplashDrone 4 (Figure 3-13).

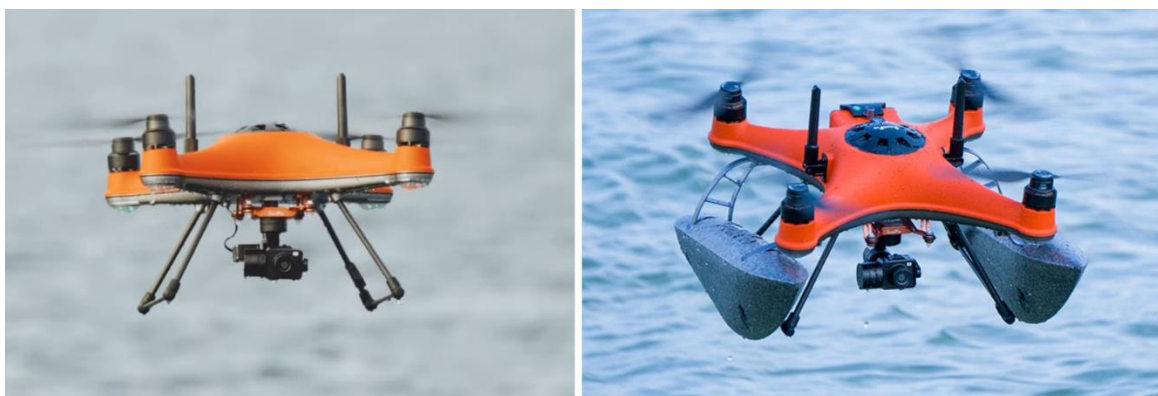


Figure 3-13: The waterproof SwellPro SplashDrone 4 (left) and setup in boat mode (right).

3.3 Depth from turbulence and surface flow characteristics

Bathymetry from surface turbulence

Another method for estimating bathymetry is from integral length scales $L_{ij,k}$ of surface turbulence (Johnson and Cowen 2016). Where $L_{11,1}$ captures the characteristic streamwise length scale of surface turbulent structures from streamwise velocity fluctuations, and $L_{22,1}$ captures the characteristic streamwise length scale of surface turbulent structures from transverse velocity fluctuations. The use of $L_{22,1}$ is generally preferred over $L_{11,1}$, since $L_{22,1}$ requires less spatial coverage (Johnson and Cowen 2016). While these methods are promising for flume data (particularly with a smooth bed), they are more challenging to apply in the field, where bathymetry is more heterogenous. It is also harder to measure high resolution surface velocities for a long duration in the field, from which integral length scales can be calculated (Detert et al. 2017). This is mainly due to practical limitations on the volumes of tracer particles that are needed to achieve high densities of surface velocities (Detert et al. 2017). Systems to artificially add tracer particles (Biggs et al. 2022) may help to overcome this limitation for small stream/ivers; however, for large rivers during floods it is unrealistic that sufficient tracer particles could be added (and for sufficient duration) to make this method feasible.

The use of advanced infrared cameras (Legleiter et al. 2017; Schweitzer and Cowen 2021) may overcome issues with tracer particle densities and recording duration that occur for introduced visible tracers. However, field tests of IR cameras by Legleiter et al. (2017) indicate that bathymetry from integral length scales of surface turbulence were outperformed by spectral methods such as Optimal Band Ratio Analysis (OBRA). Likely accuracy is influenced by the heterogeneity of depth in natural rivers (compared to flume experiments), leading to a wider range of turbulent length scales at the surface. The accuracy of these techniques may improve as the resolution and field of view of IR cameras increases (Legleiter et al. 2017).

Beyond the use of integral length scales to estimate depth, there are other surface velocimetry approaches that also show promise. For example: from surface dissipation rates of turbulent kinetic energy (Jin and Liao 2019); or the continuity equation for bathymetry over spatially heterogenous bedform models (Lin et al. 2022). While not yet operational for regular fieldwork, this is a promising area for the future, particularly for turbid flooded rivers, where optical methods requiring clear water (see Section 3.4) cannot be used. Further research is recommended to improve the understanding of the free-surface behaviour of shallow turbulent flows (Muraro et al. 2021) and improve the accuracy of bathymetry from surface velocity fields. Likewise further work is needed to improve the practicality of these methods, both for data collection with drones (e.g., flight time, coverage, and tracer densities), and for data processing.

Currently bathymetry from surface turbulence requires specialist equipment (to achieve high tracer particle densities) and specialist expertise, with data processing being challenging. The accuracy of these methods and the limitations of where they can be applied are not yet well understood. As such they are not yet suitable for practical cross section measurements during floods by council field hydrologists.

Bathymetry from surface waves

Bathymetry can also be estimated from the propagation of surface wave fields (Polcyn et al. 1970; Holman et al. 2013; Dolcetti et al. 2022). These methods were originally developed for coastal applications (Polcyn et al. 1970) but have been extended to the more complicated case of rivers (Dolcetti et al. 2022) where flow velocities are spatially heterogeneous (i.e., vertical velocity profiles

and lateral variability). Data processing can focus on the 3D water surface structure, or frequency-dependent characterisation of the wave field. Data for evaluating wave fields can be obtained in many ways, for example: single cameras (Holman et al. 2013; Dolcetti et al. 2022); stereoscopic cameras (Fedele et al. 2013); aerial laser scanners (Gorman and Hicks 2005); and microphone arrays (Dolcetti et al. 2021).

Further work is needed to develop reliable and cost effective ways to remotely measure surface wave fields. During the 'drone flow' project (Biggs 2022), tests were performed using a terrestrial laser scanner (Snoopy A-Series from LiDAR USA) to quantify water surface 3D structure. However, low numbers of returns were received from the water surface (due to penetration into the water). This is similar to the results of (Höfle et al. 2009) where high numbers of laser shot dropouts and low backscatter energy were used to classify water regions. It is unknown whether the feasibility of this technique would improve for highly turbid rivers (i.e., during large floods) or when there is a lot of floating debris and foam. The rotating LiDAR scan head also creates issues, as it does not create an instantaneous 'snapshot' of the surface structure. Instead, terrain is built up from multiple scan passes (since the data acquisition from each scan head rotation is relatively low), making it less well suited for capturing transitory terrain features (i.e., waves) with a single scan pass.

Another approach for evaluating water surface 3D structure was also tested during the drone flow project (Biggs 2022), by using a synchronous stereoscopic camera mounted on a drone. While this was more promising, the high densities of tracer particles needed for water surface reconstruction is a major limiting factor. An ideal system for 3D water surface measurements would likely be a stereoscopic camera system comprised of two high performance infrared cameras (Legleiter et al. 2017; Schweitzer and Cowen 2021). This would enable high densities of surface tracers to be achieved, without needing artificially introduced particles; however, the cost and complexity of such a system makes it unrealistic in the near term. The specialist equipment and complex data processing required for bathymetry from surface waves makes it unsuitable for practical cross section measurements during floods by council field hydrologists.

Bathymetry from flow resistance

Further methods for depth estimation have been proposed by Legleiter and Kinzel (2021) that are based on the use of a flow resistance equation. This approach is known as Depths Inferred from Velocities Estimated by Remote Sensing (DIVERS). It assumes steady, uniform, one-dimensional flow and a direct proportionality between the velocity estimated at a given location and the local water depth, with no lateral transfer of mass or momentum (Legleiter and Kinzel 2021). While further testing, validation, and potentially refinement, are needed, this method provides a plausible, first-order approximation to the reach-scale bathymetry (Legleiter and Kinzel 2021). Other related progress in this area has been made by Branch et al. (2021) to estimate bed drag coefficients from surface turbulence. Progress has also been made by Gessese et al. (2013) and others to estimate bathymetry from water surface characteristics using iterative or inverse solutions of the shallow water equations. Bathymetry from flow resistance or solving the shallow water equations could be practically applied when measurements of surface velocity distributions are available (i.e., from LSPiV); however, further work is needed to assess the accuracy of these methods and the limitations of where they can be applied. Further work is also needed to make user friendly data processing tools for use by council field hydrologists.

Summary

The estimation of depth from surface turbulence, surface waves, or flow resistance are interesting areas of research; however, application of these indirect measurement methods requires specialist expertise and often specialist equipment. Scientific progress in these areas may yield practical tools for measurement of cross sections during floods in the future, but currently the methods are not suitable for use by council field hydrologists, and other methods under development such as depth sounders towed by drones are more promising.

3.4 Optical methods (not suitable during floods)

Bathymetry from colour and spectral attenuation

Bathymetry can also be estimated from spectral information (e.g., Polcyn et al. 1970; Lyzenga 1978). These methods generally cover two key physical processes: (1) Scattering of light throughout the water column, which changes the detected 'colour' of the water as a function of depth; (2) Attenuation/absorption as a function of depth, with longer wavelengths (i.e., red to near-infrared) attenuated more rapidly than shorter wavelengths (i.e., green to blue). Bathymetry estimation from water colour and spectral attenuation has been an active area of research for a long time and has seen widespread application globally, covering diverse environments from oceans to rivers. These methods are useful for relatively clear and shallow water (Legleiter et al. 2009; Jay and Guillaume 2014; Legleiter 2016; Legleiter et al. 2018; Legleiter and Fosness 2019; Mandlbürger et al. 2021), but are limited by turbidity (optical clarity), where the signal becomes saturated beyond a certain depth, making them unsuitable for bathymetry estimation during floods. There can also be issues with shadows (Kasvi et al. 2019) and heterogenous bed cover (e.g., sediment lithology, spatial distributions of different sediment size fractions, and periphyton cover) which can complicate classifications if they have different reflectance characteristics (Winterbottom and Gilvear 1997).

These methods may be useful for remotely sensing bathymetry before or after a flood (when water is relatively clear), using software such as the Optical River Bathymetry Toolkit (Legleiter 2021). However, applying these methods usually requires multispectral aerial imagery and detailed ground truth bathymetry measurements. This makes these methods more suitable for large scale mapping of bathymetry in rivers, rather than obtaining a cross section at one location. Since these methods cannot be applied during floods due to high water turbidity (low optical clarity) they cannot capture cross sections concurrently with surface velocities, making them less suitable for application by council field hydrologists than direct measurement methods such as aerial GPR or towed depth sounders.

Bathymetry from through water imagery corrected for surface refraction

For shallow, clear water, with distinctive bottom features, bathymetry can be resolved from through water imagery corrected for surface refraction (Westaway et al. 2000 and 2001; Butler et al. 2002; Javernick et al. 2014; Woodget et al. 2015; Dietrich 2017; Mulsow et al. 2018; Skarlatos and Agrafiotis 2018; Mandlbürger 2019; Agrafiotis et al. 2020; Cao et al. 2020). These methods have been around for a long time (Tewinkel 1963; Rinner 1969; Okamoto 1984) but have gained popularity as the use of drones for aerial surveying has increased. Likewise, the ready availability of quality Structure from Motion (SfM) software such as Agisoft Metashape and Pix4D has greatly improved the practicality of dense point matching.

The use of this technique usually assumes a planar water surface, such that an underwater object (i.e., keypoint or feature) observed from two different locations and viewing angles (matched keypoint/feature), can be described by two refracted light rays that lie within two separate but

intersecting planes (Tewinkel 1963). These planes will intersect in a line that defines the 2D (i.e., XY) coordinates of the matched key point. However, the problem of depth estimation occurs because the projection of each light ray onto the other intersecting plane will occur at a different depth (for unequal viewing angles) due to refraction at the air-water interface (Dietrich 2017; Cao et al. 2020). Refraction is a function of the angle of intersection of each of the light rays with the water surface (i.e., Snell's law) (Tewinkel 1963) and the refractive index of water (Thormählen et al. 1985; Harvey et al. 1998). Refraction correction can be addressed with a range of methods, such as: simple 1D corrections for small refraction angles (Woodget et al. 2015); iterative approaches (Dietrich 2017); and methods involving the midpoint of skew lines (Cao et al. 2020). If the intrinsic and extrinsic parameters of each camera (image) are known with high precision, and the water surface equation is known/defined, then forward intersection ray tracing methods can be used (Mulsow et al. 2018), where 3D points are resolved from the closest distance between matched refracted rays. This approach is promising if a small proportion of the imagery is covered in water, such that underwater regions could be masked, and dry (terrestrial regions) used for 'optimising cameras' (i.e., calculating accurate intrinsic and extrinsic camera parameters), then forward intersection ray tracing methods used for bathymetry of the masked underwater regions. However, if the majority of the imagery is covered in water, then the problem becomes more challenging as it is very difficult to obtain accurate intrinsic and extrinsic camera parameters from underwater (refracted) key points (Mulsow et al. 2018). One major limitation of these methods is that they assume a planar water surface, whereas surface waves and spatial variability in water surface slope are common in rivers. This limitation can be overcome if a 3D model of the water surface is acquired simultaneously with the imagery collected for bathymetric mapping; however, this poses a significant technical challenge (as discussed in bathymetry from surface waves in Section 3.3).

Like bathymetry from colour and spectral attenuation, these methods may be applied to estimate the bathymetry of cross sections before or after floods; however, they are not suitable for measurements during floods that are concurrent with surface velocities due to high turbidity (low optical clarity). They also require specialist expertise, software, and data processing, making them unsuitable for routine use by council field hydrologists.

Bathymetric LiDAR

Bathymetric LiDAR is another promising technology for mapping rivers, lakes, and the coastal environment. It uses a green laser (typical wavelength of 532 nm) which penetrates clear water, compared to terrestrial LiDAR (typically near-infrared with wavelength of 1064 nm) that is rapidly absorbed by water. Bathymetric LiDAR has also been around for quite a long time; however, systems have traditionally been large, heavy, expensive, and often experimental (or with restricted access) (Hilldale and Raff 2008; Kinzel et al. 2013). The recent development of smaller light weight commercially available systems is opening up exciting possibilities for river bathymetric mapping, with some systems light enough to be deployed from drones (Mandlbürger et al. 2020; Kinzel et al. 2021; Acharya et al. 2021; Islam et al. 2022). These smaller light weight systems are also designed for deployment at low altitudes, resulting in smaller laser footprints, higher resolution, and higher point densities. This makes them better suited for mapping heterogeneous river bathymetry than traditional higher altitude bathymetric LiDAR systems deployed on manned aircraft or helicopters.

Some of the new bathymetric LiDAR systems such as the TDOT 3 Green¹⁰ and TDOT 7 Green¹¹ are very promising (Islam et al. 2022), but would benefit from more detailed independent testing of accuracy

¹⁰ <https://amuse-oneself.com/en/product/tdot3>

¹¹ <https://amuse-oneself.com/en/product/tdot3>

(Mandlbürger et al. 2020; Awadallah et al. 2023) as has been performed for the RIEGL VQ-840-G (Figure 3-14). There are also environmental limitations for the deployment of bathymetric LiDAR, notably optical clarity (turbidity)¹², and likely also water surface geometry/waves, which may decrease accuracy due to refraction at the air-water interface. It also remains to be seen how the price of these systems will change over time, as they are currently very expensive (i.e., >\$300k NZD), putting them out of the reach of most researchers or institutions. The high cost of this hardware also generates further questions as to whether it is sensible to fly them on drones. While drones are convenient to use, they do have a much higher probability of crashing than manned aircraft (e.g., hardware/software faults, pilot errors, or environmental conditions). Until these systems are available at lower prices, they are unlikely to be widely adopted for remotely sensing river bathymetry.

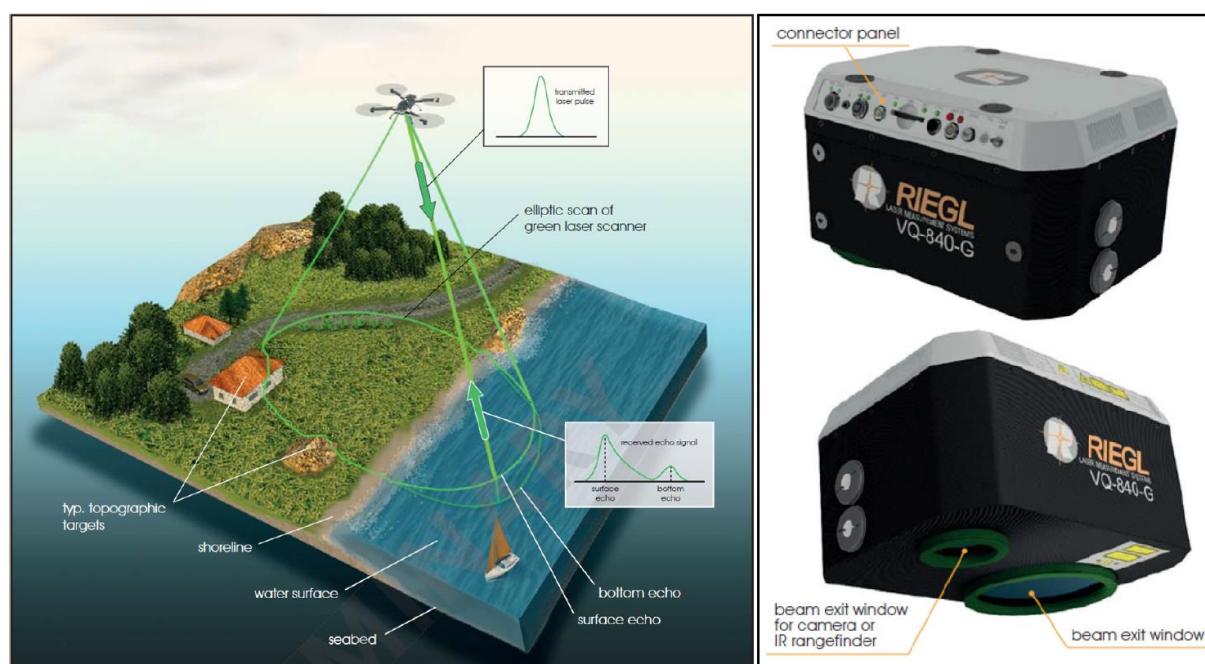


Figure 3-14: Topo-bathymetric LiDAR, showing the RIEGL VQ-840-G. Images from Mandlbürger et al. (2020).

Summary

Optical methods to estimate bathymetry may be used before or after floods; however, they are unsuitable for the measurement of cross sections during floods (i.e., concurrently with surface velocities for discharge gauging) due to high turbidity (low optical clarity). The specialist equipment/software, and specialist expertise for data processing also make these methods unsuitable for routine flood gauging measurements by council field hydrologists.

3.5 Potential future method: Estimation of cross sections during floods from before and after surveys

Cross sections are commonly surveyed before and after floods; however, there is currently little known about how they change during floods. Methods are needed to interpolate between before and after cross sections, then resample them at the time when surface velocities were recorded. Although this would not be as accurate as measuring cross sections during floods (i.e., at the same time that surface

¹² Most bathymetric LiDAR systems are limited to 1–2 Secchi depths (3 Secchi depths is quoted for Fugro RAMMS). The TDOT 3 Green and TDOT 7 Green are limited to 1.13 and 1.43 Secchi depths in clear water.

velocities were recorded), it would still provide a significant improvement in accuracy compared to assuming that the before/after cross section applied at the time surface velocities were recorded.

There are many ways that this could be achieved, ranging from simple interpolation methods, to detailed hydrodynamic and morphodynamic modelling. The approach used will be a trade-off between simplicity of implementation and accuracy of results. Likely, the optimal approach will be a combination of interpolation and simplified hydrodynamics/morphodynamics, such as using boundary shear stress as a function of discharge, coupled with estimation of particle size distributions across the cross section, to predict sediment mobility and geomorphic change for each timestep of the hydrograph. These methods are likely to be developed in the next few years and will provide an improvement over applying cross sections from before/after a flood.

4 Conclusions

The measurement of cross sections during floods still poses a technical challenge for field hydrologists globally. Where bridges or cableways are available and velocity is not extreme, weighted soundings (Section 2.1) or the Pressure Operated Electronic Meter (POEM) (Section 2.3) are still suitable measurement methods. The POEM provides superior accuracy and practicality to weighted soundings, since it does not need cable length to be measured, or corrections made for cable angle and downstream drift. However, these methods do have significant downsides, due to the time it takes to measure a cross section, and risks of submerged equipment (or the cable) becoming tangled in debris (i.e., logs).

Acoustic measurement methods using ADCPs, or depth sounders provide advantages over sounding weights and the POEM for rapid measurement of cross sections and less risk of becoming tangled in debris. They can be deployed from bridges and cableways (tethered), or alternatively on remote controlled boats or manned boats. For large floods with high concentrations of suspended sediment near the riverbed ADCPs may not be able to identify the channel bottom, and lower frequency (or dual frequency) echosounders may be needed. These echosounders are relatively cheap and robust, for example the Echologger ECT D24. The accuracy of acoustic methods for measuring cross sections is highly dependent on the accuracy of measurements of the origin and orientation of the sonar transmitter (i.e., where it is in space, and where it is pointing). ADCPs have inbuilt IMUs for orientation/tilt correction, and commonly also have GPS; however, when using custom depth sounders, it is important to ensure that tilt correction is included, and system design includes a means to accurately determine position in space (i.e., from RTK/PPK GPS). In some cases, the position of an ADCP or depth sounder across a river can be easily measured relative to a fixed point on the channel bank using a laser range finder, or by measuring the location of the tether on the bridge or cableway. For wider rivers, or where non-tethered boats are used (i.e., remote controlled or manned), then GPS will typically be needed for measurement of position. Methods for processing flood cross sections collected by moving boat ADCPs that are spatially referenced using GPS VTG strings are provided in Appendix A. Methods for processing cross sections from depth sounders that are spatially referenced using RTK GPS are provided in Appendix B.

The development and implementation of non-contact measurement methods for bathymetry is rapidly progressing (Section 3). However, many of these methods have not yet been applied to the measurement of cross sections during floods, or are unsuitable during floods due to suspended sediment and low optical clarity (i.e., optical methods in Section 3.4). The most promising methods for measurement of cross sections during floods are using ‘depth sounders on drones’ (Section 3.2) and ‘ground penetrating radar’ (Section 3.1). However, both methods still require scientific and technical development, before they are suitable for routine operations. There are currently no commercially available depth sounder systems suitable for deployment by drones to measure cross sections during large floods (i.e., suitable for high water surface velocities). There are also issues to resolve with the deployment of aerial ground penetrating radar, such as: high equipment and software costs; low flight altitudes (i.e., flight risks); specialised expertise for equipment deployment and data processing; limitations making measurements close to channel banks; and potential regulatory issues with GPR on drones if the signal is not highly directional (i.e., focused down into the river or properly shielded) and interference occurs for other radio spectrum users. A rigorous test of the accuracy of ‘depth sounders on drones’ and ‘GPR on drones’ for cross section measurements during floods, against reference bathymetry data is also needed. Until these issues are resolved, the use ‘depth sounders on drones’ or

'GPR on drones' are not yet suitable for routine use by council field hydrologists for measurement of cross sections during floods.

Similarly, non-contact measurement methods that estimate depth from turbulence and surface flow characteristics (Section 3.3) are promising, but not yet sufficiently developed, accurate, reliable, and practical, for routine use by council field hydrologists. Other approaches to estimate cross sections during floods (when surface velocities were recorded) from interpolation of before and after cross sections also require development (Section 3.5).

Currently, the most suitable methods for routine deployments are the POEM (Section 2.3) and ADCPs (Section 2.4) or depth sounders (Section 2.5). However, research on non-contact measurement methods is moving rapidly and it is likely that this report will need to be updated in the next two to three years as these technologies and methods become suitable for routine cross section measurements during floods.

5 Acknowledgements

The author would like to acknowledge valuable discussions with Martin Doyle, Graeme Smart, and Arman Haddadchi during the development of this report. The author would also like to thank Graeme Smart for his thorough review of this report. The work was funded by New Zealand's Ministry of Business, Innovation and Employment (MBIE) through the Envirolink Scheme (contract number NIW2365 2436-TSDC193), the support of which is gratefully acknowledged.

6 Glossary of abbreviations and terms

ADCP	Acoustic Doppler Current Profiler
Bathymetry	Underwater equivalent to topography (essentially a map of depth).
Discharge	The volume of water flowing down a channel each second (also known as volumetric flow rate or volumetric discharge).
Drone	Synonym for: Unmanned Aerial Vehicle (UAV), Unmanned Aerial System (UAS), Uncrewed Aerial Vehicle (UAV), and Remotely Piloted Aircraft System (RPAS). Drone is used throughout this user guide for consistency and simplicity.
Fudaa-LSPIV	Software for processing surface velocimetry videos using LSPIV.
GCP	Ground Control Point
GGA	GPS – NMEA GGA (National Marine Electronics Association - Global Positioning System Fix Data) is used for recording ADCP position; however, it is susceptible to multipath errors (particularly near banks) and requires differential correction for acceptable accuracy. Typically VTG or BT are used in New Zealand for ADCP positioning, since differential GPS corrections with SBAS (Satellite Based Augmentation System) are not yet available. However, SBAS is currently being developed in New Zealand and will be known as SouthPAN (Southern Positioning Augmentation Network) https://www.linz.govt.nz/data/geodetic-services/satellite-based-augmentation-system
Gimbal	Device under a drone that holds a camera and maintains its orientation (usually nadir/vertical) independently of the drone orientation. This avoids changes in camera orientation as the drone flies, or in response to atmospheric turbulence.
GNSS	Global Navigation Satellite System
GPR	Ground Penetrating Radar
GPS	Global Positioning System
HydroSTIV	Software for processing surface velocimetry videos using STIV or PTV.
IMU	Inertial Measurement Unit (used to measure orientation and accelerations).
LiDAR	Light Detection And Ranging is used to resolve digital elevation models of terrain at high resolution. Terrestrial LiDAR systems normally use infrared light (typical wavelength of 1064 nm), whereas bathymetric LiDAR systems use green light (typical wavelength of 532 nm, which is frequency doubled from 1064 nm). Bathymetric LiDAR systems are constantly improving; however, their high price of >\$300k NZD, limits their uptake and deployment.
LSPIV	Large Scale Particle Image Velocimetry
Nadir	Vertically oriented (i.e., parallel with the force of gravity). Nadir imagery is captured from a camera in a gimbal under an aerial vehicle to make maps.
NIWA	National Institute of Water and Atmospheric Research
OBRA	Optimal Band Ratio Analysis. This is a method for depth retrieval from the ratio of spectral bands (Legleiter 2021).
PIV	Particle Image Velocimetry (used to evaluate velocities from the motion of groups of tracer particles).
POEM	Pressure Operated Electronic Meter (for measuring depth and velocity).
PPK GPS	Post-Processed Kinematic Global Positioning System. Highly accurate GPS ~3 cm that is corrected for atmospheric distortions to GPS signal during post-processing.

PTV	Particle Tracking Velocimetry (used to evaluate velocities from the motion of individual tracer particles).
QC	Quality Control
QRev	Software for processing ADCP data developed by the USGS and Genesis HydroTech LLC. QRevInt is the international version of QRev.
RF	Radio Frequency
RIVeR	Rectification of Image Velocity Results. Software from the USGS for performing LSPIV.
RIVeR-STIV	Rectification of Image Velocity Results STIV. Software from the USGS for performing STIV.
RTK GPS	Real Time Kinematic Global Positioning System. Highly accurate GPS ~3 cm that is corrected for atmospheric distortions to GPS signal in real time. Typically this involves the deployment of a 'base station' at a known location.
Stereoscopic	Using two or more cameras to resolve depth of field in images (i.e., stereovision).
STIV	Space Time Image Velocimetry
SVR	Surface Velocity Radar
SxS Pro	Section by Section Pro is a software for measuring discharge with Teledyne RDI ADCPs using sections and is commonly used for flood gauging with moving bed.
Turbid	Murky, or not visually clear due to suspended sediment.
UAS	Unmanned Aerial System, or Uncrewed Aerial System (see 'Drone').
UAV	Unmanned Aerial Vehicle, or Uncrewed Aerial Vehicle (see 'Drone').
USGS	United States Geological Survey
VTG	GPS – NMEA VTG (National Marine Electronics Association - Track made good and ground speed) is commonly used for ADCP positioning in New Zealand. Unlike GGA it does not require differential correction and is less susceptible to multipath errors. It can also be used during mobile bed conditions when bottom track cannot. However, VTG is less accurate at slow boat speeds, which can lead to cumulative positioning errors.

7 References

- Acharya, B., Bhandari, M., Bandini, F., Pizarro, A., Perks, M., Joshi, D., Wang, S., Dogwiler, T., Ray, R., Kharel, G., Sharma, S. (2021) Unmanned aerial vehicles in hydrology and water management: Applications, challenges, and perspectives. *Water Resources Research*, 57(11).
- Agrafiotis, P., Karantzas, K., Georgopoulos, A., Skarlatos, D. (2020) Correcting image refraction: Towards accurate aerial image-based bathymetry mapping in shallow waters. *Remote Sensing*, 12(2), 322.
- Annan, A.P., Davis, J. (1977) Impulse radar applied to ice thickness measurements and freshwater bathymetry. Technical report, Current Research Part B, GSC Paper 77-1b, Geological Survey of Canada, 63–65.
- Annan, A.P. (2003) Ground penetrating radar principles, procedures and applications. *Sensors and software*, 278.
- Awadallah, M. O. M., Malmquist, C., Stickler, M., Alfredsen, K. (2023) Quantitative evaluation of bathymetric LiDAR sensors and acquisition approaches in Lærdal River in Norway. *Remote Sensing*, 15(1), 263.
- Baker, G., Jordan, T., Pardy, J. (2007) An introduction to ground penetrating radar (GPR). *Special Papers-Geological Society of America*, 432, 1-18.
- Bandini, F., Olesen, D., Jakobsen, J., Kittel, C. M. M., Wang, S., Garcia, M., Bauer-Gottwein, P. (2018) Bathymetry observations of inland water bodies using a tethered single-beam sonar controlled by an unmanned aerial vehicle. *Hydrology and Earth System Sciences*, 22(8), 4165-4181.
- Bandini, F., Kooij, L., Mortensen, B. K., Caspersen, M. B., Thomsen, L. G., Olesen, D., Bauer-Gottwein, P. (2023) Mapping inland water bathymetry with Ground Penetrating Radar (GPR) on board Unmanned Aerial Systems (UASs). *Journal of Hydrology*, 616, 128789.
- Biggs, H., Smart G., Doyle, M., Holwerda, H., McDonald, M., Ede, M. (2021) River discharge from surface velocity measurements – A field guide for selecting alpha. *Envirolink Advice Report*, Christchurch, New Zealand.
- Biggs, H., Smith, B., Detert, M., Sutton, H. (2022) Surface image velocimetry: Aerial tracer particle distribution system and techniques for reducing environmental noise with coloured tracer particles. *River Research and Applications*. 1-7.
- Biggs, H. (2022) *Drone Flow User Guide*, NIWA, Christchurch, New Zealand.
- Biggs, H., Smart, G., Doyle, M., Eickelberg, N., Aberle, J., Randall, M., Detert, M. (2023) Surface velocity to depth-averaged velocity—a review of methods to estimate alpha and remaining challenges. *Water*, 15(21), 3711.
- Branch, R., Horner-Devine, A., Chickadel, C., Talke, S., Clark, D., Jessup, A. (2021) Surface turbulence reveals riverbed drag coefficient. *Geophysical Research Letters*, 48(10), e2020GL092326.
- Butler, J., Lane, S., Chandler, J., Porfiri, E. (2002) Through-water close range digital photogrammetry in flume and field environments. *The Photogrammetric Record*, 17(99), 419-439.

- Cao, B., Deng, R., Zhu, S. (2020) Universal algorithm for water depth refraction correction in through-water stereo remote sensing. *International Journal of Applied Earth Observation and Geoinformation*, 91, 102108.
- Coppo Frias, M., Vesterhauge, A. R., Olesen, D., Bandini, F., Grosen, H., Nielsen, S., Bauer-Gottwein, P. (2024) Combining Uas Lidar, Sonar and Radar Altimetry for River Hydraulic Characterization. *Pre-print*.
- Costa, J., Spicer, K., Cheng, R., Haeni, F., Melcher, N., Thurman, E., Plant, W., Keller, W. (2000) Measuring stream discharge by non-contact methods: A proof-of-concept experiment. *Geophysical Research Letters*, 27(4), 553-556.
- Costa, J., Cheng, R., Haeni, F., Melcher, N., Spicer, K., Hayes, E., Plant, W., Hayes, K., Teague, C., Barrick, D. (2006) Use of radars to monitor stream discharge by noncontact methods. *Water Resources Research*, 42(7).
- Dawson, C. B., Lane Jr, J. W., White, E. A. (2021) Testing of sUAS ground-penetrating radar for non-contact measurement of river bathymetry. In *Symposium on the Application of Geophysics to Engineering and Environmental Problems 2021* (pp. 331-331). Society of Exploration Geophysicists and Environment and Engineering Geophysical Society.
- Detert, M., Johnson, E., Weitbrecht, V. (2017) Proof-of-concept for low-cost and non-contact synoptic airborne river flow measurements. *International Journal of Remote Sensing*, 38(8-10), 2780-2807.
- Diaz, A. L., Ortega, A. E., Tingle, H., Pulido, A., Cordero, O., Nelson, M., Ifju, P. G. (2022) The Bathy-Drone: An autonomous uncrewed drone-tethered sonar system. *Drones*, 6(10), 294.
- Dietrich, J. (2017) Bathymetric Structure-from-Motion: extracting shallow stream bathymetry from multi-view stereo photogrammetry. *Earth Surface Processes and Landforms*, 42(2), 355-364.
- Dietsch, B. J., Densmore, B. K., Strauch, K. R. (2014) Repeated multibeam echosounder hydrographic surveys of 15 selected bridge crossings along the Missouri River from Niobrara to Rulo, Nebraska, during the flood of 2011 (No. 2014-5062). US Geological Survey.
- Dolcetti, G., Alkmim, M., Cuenca, J., De Ryck, L., Krynkina, A. (2021) Robust reconstruction of scattering surfaces using a linear microphone array. *Journal of Sound and Vibration*, 494, 115902.
- Dolcetti, G., Hortobágyi, B., Perks, M., Tait, S., Dervilis, N. (2022) Using Non-contact Measurement of Water Surface Dynamics to Estimate River Discharge. *Water Resources Research*, e2022WR032829.
- Fedele, F., Benetazzo, A., Gallego, G., Shih, P. C., Yezzi, A., Barbariol, F., Ardhuin, F. (2013) Space-time measurements of oceanic sea states. *Ocean Modelling*, 70, 103-115.
- Ferguson, R. (2007) Flow resistance equations for gravel- and boulder-bed streams. *Water Resources Research*, 43(5).
- Fountain, J. (2021) Using GPS and GPS compasses with ADCPs. USGS Webinar.
- Fujita, I., Notoya, Y., Tani, K., Tateguchi, S. (2019) Efficient and accurate estimation of water surface velocity in STIV. *Environmental Fluid Mechanics*, 19(5), 1363-1378.
- Gessese, A. F., Smart, G., Heining, C., Sellier, M. (2013) One-dimensional bathymetry based on velocity measurements. *Inverse Problems in Science and Engineering*, 21(4), 704-720.

- Gorman, R., Hicks, D.M. (2005) Directional wavelet analysis of inhomogeneity in the surface wave field from aerial laser scanning data. *Journal of physical oceanography*, 35(6), 949-963.
- Guan, M., Carrivick, J. L., Wright, N. G., Sleigh, P. A., Staines, K. E. H. (2016) Quantifying the combined effects of multiple extreme floods on river channel geometry and on flood hazards. *Journal of Hydrology*, 538, 256-268.
- Harvey, A., Gallagher, J., Sengers, J. (1998) Revised formulation for the refractive index of water and steam as a function of wavelength, temperature and density. *Journal of Physical and Chemical Reference Data*, 27(4), 761-774.
- Hilldale, R., Raff, D. (2008) Assessing the ability of airborne LiDAR to map river bathymetry. *Earth Surface Processes and Landforms*, 33(5), 773-783.
- Höfle, B., Vetter, M., Pfeifer, N., Mandlbürger, G., Stötter, J. (2009) Water surface mapping from airborne laser scanning using signal intensity and elevation data. *Earth Surface Processes and Landforms*, 34(12), 1635-1649.
- Holman, R., Plant, N., Holland, T. (2013) cBathy: A robust algorithm for estimating nearshore bathymetry. *Journal of geophysical research: Oceans*, 118(5), 2595-2609.
- Hong, J., Guo, W., Wang, H., Yeh, P. (2017) Estimating discharge in gravel-bed river using non-contact ground-penetrating and surface-velocity radars. *River Research and Applications*, 33(7), 1177-1190.
- Hydro Technology Institute (2022) *Hydro-STIV Operation Manual*. Osaka, Japan.
- Islam, M., Yoshida, K., Nishiyama, S., Sakai, K., Tsuda, T. (2022) Characterizing vegetated rivers using novel unmanned aerial vehicle-borne topo-bathymetric green lidar: Seasonal applications and challenges. *River Research and Applications*, 38(1), 44-58.
- ISO748 (2007) *Hydrometry – Measurement of liquid flow in open channels using current meters or floats*.
- Javernick, L., Brasington, J., Caruso, B. (2014) Modeling the topography of shallow braided rivers using Structure-from-Motion photogrammetry. *Geomorphology*, 213, 166-182.
- Jay, S., Guillaume, M. (2014) A novel maximum likelihood based method for mapping depth and water quality from hyperspectral remote-sensing data. *Remote sensing of environment*, 147, 121-132.
- Jin, T., Liao, Q. (2019) Application of large-scale PIV in river surface turbulence measurements and water depth estimation. *Flow Measurement and Instrumentation*, 67, 142-152.
- Jodeau, M., Hauet, A., Le Coz, J., Bodart, G. (2019) *Fudaa-LSPIV Version 1.7. 1 User Manual*. Lyon: IRSTEA France.
- Johnson, E., Cowen, E. (2016) Remote monitoring of volumetric discharge employing bathymetry determined from surface turbulence metrics. *Water Resources Research*, 52(3), 2178-2193.
- Kasvi, E., Salmela, J., Lotsari, E., Kumpula, T., Lane, S. (2019) Comparison of remote sensing based approaches for mapping bathymetry of shallow, clear water rivers. *Geomorphology*, 333, 180-197.

- Kinzel, P., Legleiter, C., Nelson, J. (2013) Mapping river bathymetry with a small footprint green LiDAR: applications and challenges 1. *JAWRA Journal of the American Water Resources Association*, 49(1), 183-204.
- Kinzel, P., Legleiter, C., Grams, P. (2021) Field evaluation of a compact, polarizing topo-bathymetric lidar across a range of river conditions. *River Research and Applications*, 37(4), 531-543.
- Koutalakis, P., Zaimis, G. N. (2022) River flow measurements utilizing UAV-based surface velocimetry and bathymetry coupled with sonar. *Hydrology*, 9(8), 148.
- Lane, J., Dawson, C., White, E., Fulton, J. (2020) Non-contact measurement of river bathymetry using sUAS Radar: Recent developments and examples from the Northeastern United States. In proceedings of the Fifth International Conference on Engineering Geophysics (ICEG), Al Ain, United Arab Emirates.
- Le Coz, J., Hauet, A., Pierrefeu, G., Dramais, G., Camenen, B. (2010) Performance of image-based velocimetry (LSPIV) applied to flash-flood discharge measurements in Mediterranean rivers. *Journal of hydrology*, 394(1-2), 42-52.
- Legleiter, C., Roberts, D., Lawrence, R. (2009) Spectrally based remote sensing of river bathymetry. *Earth Surface Processes and Landforms*, 34(8), 1039-1059.
- Legleiter, C. (2016) Inferring river bathymetry via image-to-depth quantile transformation (IDQT). *Water Resources Research*, 52(5), 3722-3741.
- Legleiter, C., Kinzel, P., Nelson, J. (2017) Remote measurement of river discharge using thermal particle image velocimetry (PIV) and various sources of bathymetric information. *Journal of Hydrology*, 554, 490-506.
- Legleiter, C., Overstreet, B., Kinzel, P. (2018) Sampling strategies to improve passive optical remote sensing of river bathymetry. *Remote Sensing*, 10(6), 935.
- Legleiter, C., Fosness, R. (2019) Defining the limits of spectrally based bathymetric mapping on a large river. *Remote Sensing*, 11(6), 665.
- Legleiter, C. (2021) The optical river bathymetry toolkit. *River Research and Applications*, 37(4), 555-568.
- Legleiter, C., Kinzel, P. (2021) Depths Inferred from Velocities Estimated by Remote Sensing: A Flow Resistance Equation-Based Approach to Mapping Multiple River Attributes at the Reach Scale. *Remote Sensing*, 13(22), 4566.
- Legleiter, C.J., Kinzel, P.J. (2023) The toolbox for river velocimetry using images from aircraft (TRiVIA). *River Research and Applications*, 39(8), 1457-1468.
- Lin, Y., Ho, H., Lee, T., Chen, H. (2022) Application of Image Technique to Obtain Surface Velocity and Bed Elevation in Open-Channel Flow. *Water*, 14(12), 1895.
- Lyzenga, D. (1978) Passive remote sensing techniques for mapping water depth and bottom features. *Applied optics*, 17(3), 379-383.
- Mandlburger, G. (2019) Through-water dense image matching for shallow water bathymetry. *Photogrammetric Engineering & Remote Sensing*, 85(6), 445-455.

- Mandlburger, G., Pfennigbauer, M., Schwarz, R., Flöry, S., Nussbaumer, L. (2020) Concept and performance evaluation of a novel UAV-borne topo-bathymetric LiDAR sensor. *Remote Sensing*, 12(6), 986.
- Mandlburger, G., Kölle, M., Nübel, H., Soergel, U. (2021) BathyNet: A deep neural network for water depth mapping from multispectral aerial images. *ISPRS – Journal of Photogrammetry, Remote Sensing and Geoinformation Science*, 89(2), 71-89.
- McMillan, H., Freer, J., Pappenberger, F., Krueger, T., Clark, M. (2010) Impacts of uncertain river flow data on rainfall-runoff model calibration and discharge predictions. *Hydrological Processes*, 24(10), 1270-1284.
- Melcher, N., Costa, J., Haeni, F., Cheng, R., Thurman, E., Buursink, M., Spicer, K., Hayes, E., Plant, W., Keller, W., Hayes, K. (2002) River discharge measurements by using helicopter-mounted radar. *Geophysical Research Letters*, 29(22), 41-1.
- Muraro, F., Dolcetti, G., Nichols, A., Tait, S., Horoshenkov, K. (2021) Free-surface behaviour of shallow turbulent flows. *Journal of Hydraulic Research*, 59(1), 1-20.
- Mulsow, C., Kenner, R., Bühler, Y., Stoffel, A., Maas, H. (2018) Subaquatic digital elevation models from UAV-imagery. *International Archives of the Photogrammetry, Remote Sensing & Spatial Information Sciences*, 42(2).
- Muste, M., Fujita, I., Hauet, A. (2008) Large-scale particle image velocimetry for measurements in riverine environments. *Water Resources Research*, 44(4), 1-14.
- NEMS (2013) Open Channel Flow Measurement. New Zealand National Environmental Monitoring Standards.
- Nikora, V. I., Smart, G. M. (1997) Turbulence characteristics of New Zealand gravel-bed rivers. *Journal of Hydraulic Engineering*, 123(9), 764-773.
- Okamoto, A. (1984) Orientation problem of two media photographs with curved boundary surfaces. *Photogrammetric engineering and remote sensing*, 50(3), 303-316.
- Patalano, A., García, C., Rodríguez, A. (2017) Rectification of Image Velocity Results (RIVeR): A simple and user-friendly toolbox for large scale water surface Particle Image Velocimetry (PIV) and Particle Tracking Velocimetry (PTV). *Computers & Geosciences*, 109, 323-330.
- Polcyn, F., Brown, W., Sattinger, I. (1970) The measurement of water depth by remote sensing techniques. Report for the Spacecraft Oceanography Project, The University of Michigan, Ann Arbor, Michigan.
- Randall, M. (2021) National Industry Guidelines for hydrometric monitoring – Part 11: Application of surface velocity methods for velocity and open channel discharge measurements. Bureau of Meteorology, Melbourne, Australia.
- Rantz, S. (1982) Measurement and computation of stream-flow: Measurement of stage and discharge. U.S. Geological Survey Water Supply Paper 2175.
- Rehmel, M. (2013) GPS best practices for moving-boat ADCP measurements. USGS Webinar.

- Rickenmann, D., Badoux, A., Hunzinger, L. (2016) Significance of sediment transport processes during piedmont floods: the 2005 flood events in Switzerland. *Earth Surface Processes and Landforms*, 41(2), 224-230.
- Rinner, K. (1969) Two Media Photogrammetry. *Photogrammetric Engineering*, Vol. 35, pp. 275-282.
- Rossi, L., Mammi, I., Pelliccia, F. (2020) UAV-derived multispectral bathymetry. *Remote Sensing*, 12(23), 3897.
- Schweitzer, S., Cowen, E. (2021) Instantaneous River-Wide Water Surface Velocity Field Measurements at Centimeter Scales Using Infrared Quantitative Image Velocimetry. *Water Resources Research*, 57(8), 1-28.
- Skarlatos, D., Agrafiotis, P. (2018) A novel iterative water refraction correction algorithm for use in structure from motion photogrammetric pipeline. *Journal of Marine Science and Engineering*, 6(3), 77.
- Smart, G. M. (1991) A POEM on the Waiho (electronic gauging of rivers). *Journal of Hydrology (New Zealand)*, 37-44.
- Spicer, K., Costa, J., Placzek, G. (1997) Measuring flood discharge in unstable stream channels using ground-penetrating radar. *Geology*, 25(5), 423-426.
- Tewinkel, G. (1963) Water depths from aerial photographs. *Photogrammetric Engineering*, 29(6), 1037-1042.
- Thormählen, I., Straub, J., Grigull, U. (1985) Refractive index of water and its dependence on wavelength, temperature, and density. *Journal of physical and chemical reference data*, 14(4), 933-945.
- Turnipseed, D.P., Sauer, V. (2010) Discharge measurements at gaging stations (No. 3-A8). United States Geological Survey.
- Wagner, C., Mueller, D. (2011) Comparison of bottom-track to global positioning system referenced discharges measured using an acoustic Doppler current profiler. *Journal of Hydrology*, 401(3-4), 250-258.
- Welber, M., Le Coz, J., Laronne, J., Zolezzi, G., Zamler, D., Dramais, G., Hauet, A., Salvaro, M. (2016) Field assessment of noncontact stream gauging using portable surface velocity radars (SVR). *Water Resources Research*, 52(2), 1108-1126.
- Westaway, R., Lane, S., Hicks, D.M. (2000) The development of an automated correction procedure for digital photogrammetry for the study of wide, shallow, gravel-bed rivers. *Earth Surface Processes and Landforms*, 25(2), 209-226.
- Westaway, R., Lane, S., Hicks, D.M. (2001) Remote sensing of clear-water, shallow, gravel-bed rivers using digital photogrammetry. *Photogrammetric Engineering and Remote Sensing*, 67(11), 1271-1282.
- Williams, R. D., Rennie, C. D., Brasington, J., Hicks, D. M., Vericat, D. (2015) Linking the spatial distribution of bed load transport to morphological change during high-flow events in a shallow braided river. *Journal of Geophysical Research: Earth Surface*, 120(3), 604-622.

- Woodget, A., Dietrich, J., Wilson, R. (2019) Quantifying below-water fluvial geomorphic change: The implications of refraction correction, water surface elevations, and spatially variable error. *Remote Sensing*, 11(20), 2415.
- Wyżga, B., Zawiejska, J., Radecki-Pawlik, A. (2016) Impact of channel incision on the hydraulics of flood flows: Examples from Polish Carpathian rivers. *Geomorphology*, 272, 10-20.
- Yadav, A., Sen, S., Mao, L., Schwanghart, W. (2022) Evaluation of flow resistance equations for high gradient rivers using geometric standard deviation of bed material. *Journal of Hydrology*, 605, 127292.

Appendix A Cross sections from moving boat ADCP gaugings

Cross sections from moving boat ADCP gaugings (Section 2.4) can be exported from QRev¹³ (or QRevInt¹⁴), or generated using a tool from the 'drone flow' software toolbox (Biggs 2022). This appendix provides further information on how to accomplish this.

Cross sections from QRev

In QRev data should be pre-processed and quality controlled, with only good transects that will be used for the output cross section selected. The navigation reference should be set to VTG if there are mobile bed conditions (typical of flood cross sections) as bottom track will not provide accurate data. In the MAP tab of QRev the average cross section of the selected transects can be visualised, then data exported as a .csv file (Figure A-1).

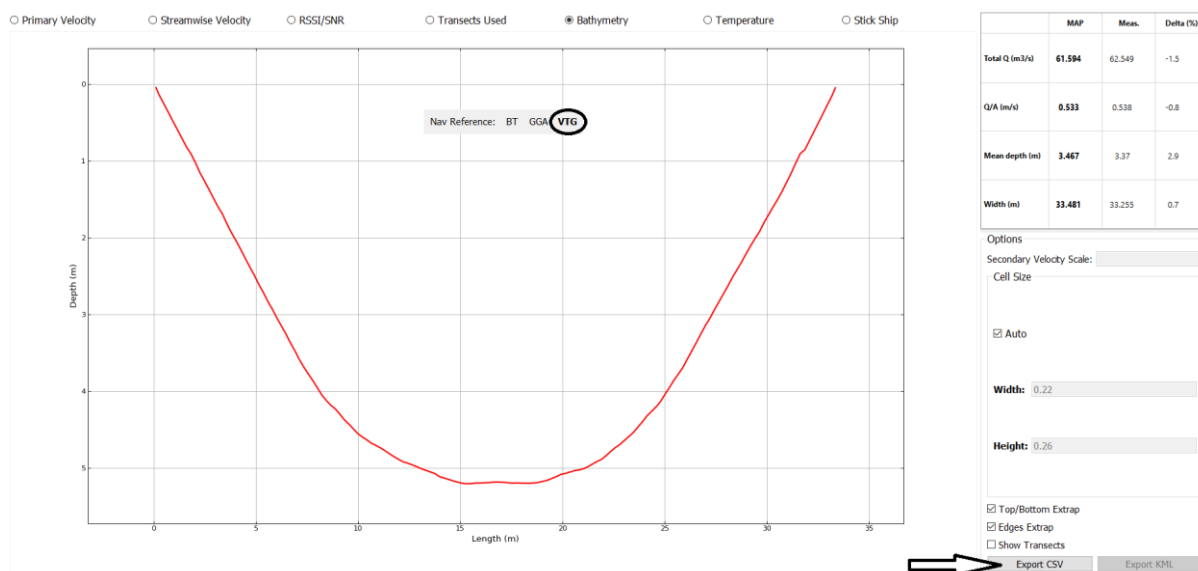


Figure A-1: Exporting bathymetry from the MAP tab of QRev. Navigation reference needs to be set to VTG for flood measurements with mobile bed sediment.

The .csv file of data exported from QRev (Figure A-2) contains a lot of additional data, beyond cross stream displacement and depth (highlighted in Figure A-2). The exported file also contains duplicate rows of data that need to be removed. To remove duplicate rows, select data in the 'Distance (Left Bank) (m)' column, then click 'Remove Duplicates' in the 'Data' tab of excel, and check 'Expand the selection' (Figure A-2). In the next dialogue box that appears only check 'Distance (Left Bank) (m)' for removing duplicates (Figure A-3). This will then remove the duplicate rows, providing cross section data that is ready to export (Figure A-4).

¹³ <https://hydroacoustics.usgs.gov/movingboat/QRev.shtml#Download>

¹⁴ <https://www.geneshydrotech.com/qrevint>

Microsoft Excel interface showing a data table with a 'Remove Duplicates' dialog box open. The dialog box is set to 'Expand the selection' and 'Continue with the current selection'. The table contains columns for various measurements like Distance, Latitude, Longitude, etc. A red circle highlights the 'Remove Duplicates' button in the ribbon.

Vertical	Distance (Left bank) (m)	Distance X (m)	Distance Y (m)	Latitude	Longitude	Primary vs Secondary	Streamwise Transvers	Vertical vs Depth (m)	Cells disc	Cells area	Distance (Depth cell)	Temperat	RSSI (cour	Nb. of Transsects
2	0.50606753	-0.16237838	0.594736096	0.139687	-0.00759	0.138268	0.021262	0.139687	0.256643184	0.007515	0.054352	0.508969	0.145727	
3	0.947815294	-0.278728365	1.020886033	0.147964	-0.01125	0.146146	0.025714	0.147964	0.480667738	0.006983	0.047782	0.966482	0.401732	
4	1.610436941	-0.453253343	1.660110938	0.265301	-0.04116	0.259983	0.066987	0.265301	0.81670457	0.015129	0.058311	1.610437	0.132	11.60375 86.0625 4
5	1.610436941	-0.453253343	1.660110938	0.265505	-0.04869	0.259447	0.074506	0.265505	0.81670457	0.015129	0.058311	1.610437	0.396	11.60375 91.53125 4
6	1.610436941	-0.453253343	1.660110938	0.22662	0.089845	0.234342	-0.06718	0.22662	0.81670457	0.013665	0.058311	1.610437	0.66	11.60375 136.0938 4
7	1.610436941	-0.453253343	1.660110938	0.103953	0.089845	0.112267	-0.07921	0.103953	0.81670457	0.000613	0.005457	1.610437	0.804352	11.60375 0
8	1.831310823	-0.511428336	1.873185906	0.272658	0.014919	0.26967	0.04293	0.272658	0.906946781	0.015725	0.058311	1.831311	0.132	11.60375 84.53125 4
9	1.831310823	-0.511428336	1.873185906	0.217773	0.014529	0.215937	0.031735	0.217773	0.906946781	0.012591	0.058311	1.831311	0.396	11.60375 90.8125 4
10	1.831310823	-0.511428336	1.873185906	0.323288	-0.02945	0.309802	0.096979	0.323288	0.906946781	0.018065	0.058311	1.831311	0.66	11.60375 100.375 4
11	1.831310823	-0.511428336	1.873185906	0.208134	-0.02945	0.197239	0.072689	0.208134	0.906946781	0.005008	0.025389	1.831311	0.849473	11.60375 0
12	2.052184706	-0.569603329	2.086260874	0.358276	-0.03046	0.359536	0.004856	0.358276	1.022924121	0.020965	0.058311	2.052185	0.132	11.58625 84.5625 4
13	2.052184706	-0.569603329	2.086260874	0.341983						0.058311	2.052185	0.396	11.58625 91.46875 4	
14	2.052184706	-0.569603329	2.086260874	0.253613						0.058311	2.052185	0.66	11.58625 89.625 4	
15	2.052184706	-0.569603329	2.086260874	0.187173						0.051005	2.052185	0.907462	11.58625 0	
16	2.273058588	-0.627778321	2.299335843	0.435758						0.058311	2.273059	0.132	11.595 83.28125 4	
17	2.273058588	-0.627778321	2.299335843	0.367742						0.058311	2.273059	0.396	11.595 85.875 4	
18	2.273058588	-0.627778321	2.299335843	0.39077						0.058311	2.273059	0.66	11.595 86.78125 4	
19	2.273058588	-0.627778321	2.299335843	0.379855						0.058311	2.273059	0.924	11.595 96.75 3	
20	2.273058588	-0.627778321	2.299335843	0.226262						0.021742	2.273059	1.105218	11.595 0	
21	2.49393247	-0.685953314	2.512410811	0.39067						0.058311	2.493932	0.132	11.56 81.5625 4	
22	2.49393247	-0.685953314	2.512410811	0.423471	0.005552	0.422723	0.025765	0.423471	1.26329881	0.024649	0.058311	2.493932	0.396	11.56 87.03125 4
23	2.49393247	-0.685953314	2.512410811	0.428553	-0.02071	0.42585	0.052327	0.428553	1.26329881	0.024832	0.058311	2.493932	0.66	11.56 85.4375 4
24	2.49393247	-0.685953314	2.512410811	0.378719	0.028114	0.379761	-4.23E-05	0.378719	1.26329881	0.022144	0.058311	2.493932	0.924	11.56 84.90625 4
25	2.49393247	-0.685953314	2.512410811	0.259186	0.028114	0.260555	-0.00888	0.259186	1.26329881	0.01193	0.045787	2.493932	1.159649	11.56 0
26	2.714806353	-0.744128307	2.725485779	0.41705	0.023295	0.417056	-0.0232	0.41705	1.371457319	0.024319	0.058311	2.714806	0.132	11.5775 83.375 4
27	2.714806353	-0.744128307	2.725485779	0.420363	0.009963	0.420366	-0.00987	0.420363	1.371457319	0.024512	0.058311	2.714806	0.396	11.5775 81.53125 4
28	2.714806353	-0.744128307	2.725485779	0.392643	-0.00846	0.392641	0.008551	0.392643	1.371457319	0.022895	0.058311	2.714806	0.66	11.5775 80.625 4
29	2.714806353	-0.744128307	2.725485779	0.403071	-0.02659	0.403065	0.02658	0.403071	1.371457319	0.023503	0.058311	2.714806	0.924	11.5775 79.15625 4
30	2.714806353	-0.744128307	2.725485779	0.359808	0.001791	0.359808	-0.00171	0.359808	1.371457319	0.020981	0.058311	2.714806	1.188	11.5775 96.6875 3
31	2.714806353	-0.744128307	2.725485779	0.173678	0.001791	0.173679	-0.00175	0.173678	1.371457319	0.001974	0.011366	2.714806	1.345729	11.5775 0
32	2.935680235	-0.802303299	2.938560747	0.403849	0.008025	0.403865	-0.01043	0.403849	1.486379475	0.023539	0.058311	2.93568	0.132	11.58625 83.78125 4
33	2.935680235	-0.802303299	2.938560747	0.40577	0.017841	0.40546	-0.02387	0.40577	1.486379475	0.023643	0.058311	2.93568	0.396	11.58625 81.875 4
34	2.935680235	-0.802303299	2.938560747	0.419067	0.012941	0.418833	-0.01887	0.419067	1.486379475	0.024422	0.058311	2.93568	0.66	11.58625 79.75 4
35	2.935680235	-0.802303299	2.938560747	0.418538	-0.02687	0.418699	0.007739	0.418538	1.486379475	0.024415	0.058311	2.93568	0.924	11.58625 79.3125 4
36	2.935680235	-0.802303299	2.938560747	0.403393	-0.02454	0.403713	0.018537	0.403393	1.486379475	0.023541	0.058311	2.93568	1.188	11.58625 81.875 4
37	2.935680235	-0.802303299	2.938560747	0.252184	-0.02454	0.252522	0.020786	0.252184	1.486379475	0.00928	0.036749	2.93568	1.40319	11.58625 0
38	3.156554117	-0.860478292	3.151635716	0.377505	0.007799	0.375701	-0.03768	0.377505	1.598971766	0.021907	0.058311	3.156554	0.132	11.595 84.15625 4

Figure A-2: Data exported from QRev MAP tab as a .csv file. Duplicate rows need to be removed.

Microsoft Excel interface showing the same data table as Figure A-2, but with the 'Remove Duplicates' dialog box open. The 'Distance (Left bank) (m)' column is selected in the 'Columns' list. The dialog box is set to 'Expand the selection' and 'Continue with the current selection'.

Vertical	Distance (Left bank) (m)	Distance X (m)	Distance Y (m)	Latitude	Longitude	Primary vs Secondary	Streamwise Transvers	Vertical vs Depth (m)	Cells disc	Cells area	Distance (Depth cell)	Temperat	RSSI (cour	Nb. of Transsects averaged
2	0.50606753	-0.16237838	0.594736096	0.139687	-0.00759	0.138268	0.021262	0.139687	0.256643184	0.007515	0.054352	0.508969	0.145727	
3	0.947815294	-0.278728365	1.020886033	0.147964	-0.01125	0.146146	0.025714	0.147964	0.480667738	0.006983	0.047782	0.966482	0.401732	
4	1.610436941	-0.453253343	1.660110938	0.265301	-0.04116	0.259983	0.066987	0.265301	0.81670457	0.015129	0.058311	1.610437	0.132	11.60375 86.0625 4
5	1.610436941	-0.453253343	1.660110938	0.265505	-0.04869	0.259447	0.074506	0.265505	0.81670457	0.015129	0.058311	1.610437	0.396	11.60375 91.53125 4
6	1.610436941	-0.453253343	1.660110938	0.22662	0.089845	0.234342	-0.06718	0.22662	0.81670457	0.013665	0.058311	1.610437	0.66	11.60375 136.0938 4
7	1.610436941	-0.453253343	1.660110938	0.103953	0.089845	0.112267	-0.07921	0.103953	0.81670457	0.000613	0.005457	1.610437	0.804352	11.60375 0
8	1.831310823	-0.511428336	1.873185906	0.272658	0.014919	0.26967	0.04293	0.272658	0.906946781	0.015725	0.058311	1.831311	0.132	11.60375 84.53125 4
9	1.831310823	-0.511428336	1.873185906	0.217773	0.014529	0.215937	0.031735	0.217773	0.906946781	0.012591	0.058311	1.831311	0.396	11.60375 90.8125 4
10	1.831310823	-0.511428336	1.873185906	0.323288	-0.02945	0.309802	0.096979	0.323288	0.906946781	0.018065	0.058311	1.831311	0.66	11.60375 100.375 4
11	1.831310823	-0.511428336	1.873185906	0.208134	-0.02945	0.197239	0.072689	0.208134	0.906946781	0.005008	0.025389	1.831311	0.849473	11.60375 0
12	2.052184706	-0.569603329	2.086260874	0.358276	-0.03046	0.359536	0.004856	0.358276	1.022924121	0.020965	0.058311	2.052185	0.132	11.58625 84.5625 4
13	2.052184706	-0.569603329	2.086260874	0.341983						0.058311	2.052185	0.396	11.58625 91.46875 4	
14	2.052184706	-0.569603329	2.086260874	0.253613						0.058311	2.052185	0.66	11.58625 89.625 4	
15	2.052184706	-0.569603329	2.086260874	0.187173						0.051005	2.052185	0.907462	11.58625 0	
16	2.273058588	-0.627778321	2.299335843	0.435758						0.058311	2.273059	0.132	11.595 83.28125 4	
17	2.273058588	-0.627778321	2.299335843	0.367742						0.058311	2.273059	0.396	11.595 85.875 4	
18	2.273058588	-0.627778321	2.299335843	0.39077						0.058311	2.273059	0.66	11.595 86.78125 4	
19	2.273058588	-0.627778321	2.299335843	0.379855						0.058311	2.273059	0.924	11.595 96.75 3	
20	2.273058588	-0.627778321	2.299335843	0.226262						0.021742	2.273059	1.105218	11.595 0	
21	2.49393247	-0.685953314	2.512410811	0.39067						0.058311	2.493932	0.132	11.56 81.5625 4	
22	2.49393247	-0.685953314	2.512410811	0.423471	0.005552	0.422723	0.025765	0.423471	1.26329881	0.024649	0.058311	2.493932	0.396	11.56 87.03125 4
23	2.49393247	-0.685953314	2.512410811	0.428553	-0.02071	0.42585	0.052327	0.428553	1.26329881	0.024832	0.058311	2.493932	0.66	11.56 85.4375 4
24	2.49393247	-0.685953314	2.512410811	0.378719	0.028114	0.379761	-4.23E-05	0.378719	1.26329881	0.022144	0.058311	2.493932	0.924	11.56 84.90625 4
25	2.49393247	-0.685953314	2.512410811	0.259186	0.028114	0.260555	-0.00888	0.259186	1.26329881	0.01193	0.045787	2.493932	1.159649	11.56 0
26	2.714806353	-0.744128307												

Vertical	Distance (Left bank) (m)	Distance X (m)	Distance Y (m)	Latitude	Longitude	Primary vs Secondary	Streamwidth	Transvers	Vertical vs Depth (m)	Cells disc	Cells area	Distance	Depth cell	Temperat	RSSI	(cour	Nb. of	Transects av
2	0.50606753	-0.16237838	0.594736096															
4	0.947815294	-0.278728365	1.020886033															
7	1.610436941	-0.453253343	1.660110938															
8	1.831310823	-0.511428396	1.873185906															
9	2.052184706	-0.569603329	2.086260874															
10	2.273058588	-0.627778321	2.299335843															
11	2.49393247	-0.685953314	2.512410811															
12	2.714806353	-0.744133007	2.725485779															
13	2.935680235	-0.802303299	2.938560747															
14	3.156554117	-0.860478292	3.151635716															
15	3.377428	-0.918653285	3.364710684															
16	3.598301882	-0.976828278	3.577785652															
17	3.819175764	-1.03503027	3.790860621															
18	4.040049647	-1.093178263	4.003935589															
19	4.260923529	-1.15133256	4.217010557															
20	4.481797411	-1.209528248	4.430085525															
21	4.702671293	-1.267703241	4.643160494															
22	4.923545176	-1.325878234	4.856235462															
23	5.144419058	-1.384053227	5.06931043															
24	5.36529294	-1.442228219	5.282385399															
25	5.586166823	-1.500403212	5.495460367															
26	5.807040705	-1.558578205	5.708535335															
27	6.027914587	-1.616753197	5.921610303															
28	6.24879847	-1.67492819	6.134685272															
29	6.46962352	-1.733103183	6.34776024															
30	6.690536234	-1.791278176	6.560835208															
31	6.911410117	-1.849453168	6.773910177															
32	7.132283999	-1.907628161	6.986985145															
33	7.353157881	-1.965803154	7.200060113															
34	7.574031763	-2.023978146	7.413135081															
35	7.794905646	-2.082153139	7.62621005															
36	8.015779528	-2.140328132	7.839285018															
37	8.23665341	-2.198503125	8.052359986															
38	8.457527293	-2.256678117	8.265434955															
39	8.678401175	-2.31485311	8.478509923															
40	8.899275057	-2.373028103	8.691584891															
41	9.12014694	-2.431203095	8.904659859															

Figure A-4: Data from QRev after removing duplicate rows. The 'Distance (Left bank) (m)' and 'Depth (m)' columns can now be used to generate a cross section file.

Following removal of duplicate values, data can be copied to a new .csv cross section file. For the surface velocimetry software Hydro-STIV the standard input format is a column labelled length (i.e., cross stream displacement from the left bank in metres) and a column labelled height (Figure A-5). The depth values exported from QRev should be converted to negative heights (i.e., minus depth), and the extrapolated riverbanks are manually added (highlighted in Figure A-5) from the MAP tab of QRev (i.e., 0,0 and Width (m), 0), see Figure A-1.

	A	B
1	Length	Height
2	0	0
3	0.50606753	-0.256643184
4	0.947815294	-0.480667738
5	1.610436941	-0.81670457
6	1.831310823	-0.906946781
7	2.052184706	-1.022924121
8	2.273058588	-1.1544366
9	2.49393247	-1.26329881
10	2.714806353	-1.371457319
11	2.935680235	-1.486379475
12	3.156554117	-1.598971766
13	3.377428	-1.694146871
14	3.598301882	-1.82419494
15	3.819175764	-1.93792502
16	4.040049647	-2.041346951
...		
141	31.64928494	-0.902403501
142	31.87015882	-0.854687076
143	32.0910327	-0.73746544
144	32.53278046	-0.503022169
145	32.97452823	-0.268578897
146	33.481	0
147		

Figure A-5: Cross section .csv file for use in Hydro-STIV. Extrapolation to riverbanks needs to be manually added as it is not exported from the MAP tab of QRev. Depth is also converted to negative height values.

Cross sections using 'drone flow' software tool

Cross sections from moving boat ADCP gaugings can also be generated using a software tool developed by the 'drone flow' project (Biggs 2022). This software utilises QRev (or QRevInt) for ADCP data pre-processing, and then extracts relevant data from the .mat file that is saved by QRev.

The software first plots the individual transect displacements with the available distance references (Figure A-1: Left). The software then projects the 2D displacement (solid lines) onto the 1D transect (dashed lines) in Figure A-1: Left. It then sorts the depth data by linear displacement and resamples it with linear interpolation (Figure A-1: Right). This accounts for the boat path and will remove any loops in the data.

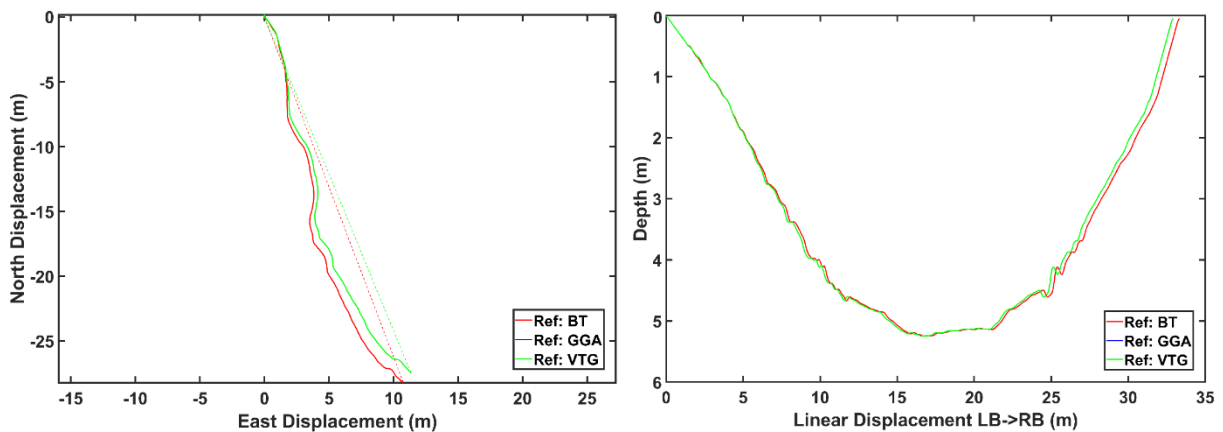


Figure A-1: Left: ADCP displacement during a transect. Right: Cross section after vector projection of North/East displacement onto cross section unit vector, and resampling (linear interpolation) of depth.

After plotting depth vs linear displacement (Figure A-1: Right), any differences between the distance references will become visible (i.e., drift/divergence). The next step is to select which distance reference to use, or to manually enter the cross section width. Manual cross section widths are useful if the cross section width has been measured accurately (i.e., surveyed with RTK GPS), or if the ADCP has tracked a diagonal path across the channel (creating a longer cross section than one orthogonal to the banks).

When choosing a distance reference, it is important to understand that although the established methods generally perform well, there is no 'perfect solution' and limitations should be understood (Wagner and Mueller 2011; Rehmel 2013; Fountain 2021). For example:

- GPS – NMEA GGA (National Marine Electronics Association - Global Positioning System Fix Data) is susceptible to multipath errors (particularly near banks) and requires differential correction for acceptable accuracy.
- GPS – NMEA VTG (National Marine Electronics Association - Track made good and ground speed) is less accurate at slow boat speeds (cumulative errors). However, it does not require differential correction and is less susceptible to multipath errors.
- BT (Bottom track) doesn't work for moving bed conditions.
- GPS – RTK (Real Time Kinematic) or PPK (Post Processed Kinematic) requires specialist equipment and setup.

Typically VTG or BT are used in New Zealand, since differential GPS corrections with SBAS (Satellite Based Augmentation System) are not yet available¹⁵. For flood cross sections there will typically be moving bed conditions, so VTG should be used rather than bottom track. Once the distance reference has been selected, all of the available linear displacement measurements will be rescaled to this distance reference to remove cumulative drift in the measurements (Figure A-2: Left). Next, the user can elect to use the selected distance reference transect width, or they can manually enter transect width if it has been accurately measured. Finally, all of the transects are overlain (Figure A-2: Right), then the user can select which transects to be included in the final output (i.e., to remove any outliers), with the select transects then averaged and exported as a .csv file.

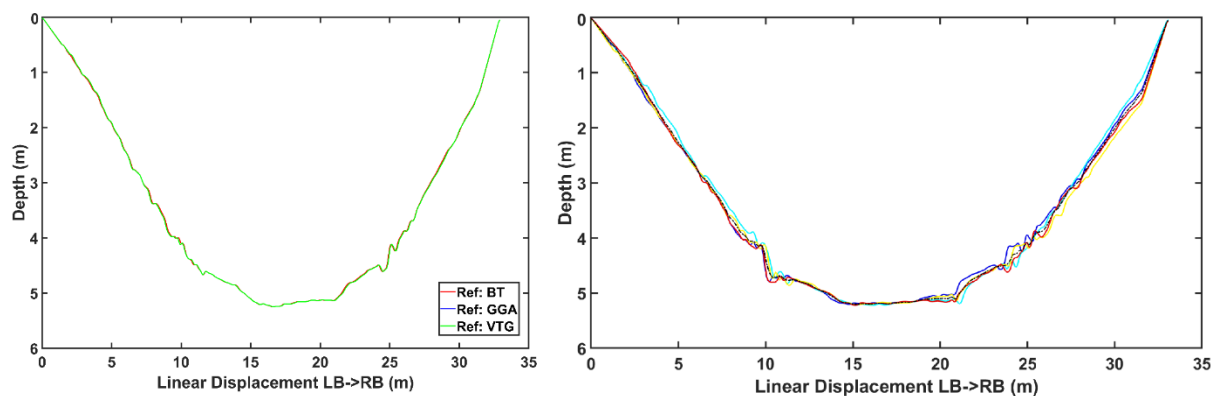


Figure A-2: Left: Rescaling of linear displacement to account for drift in distance sources. Width can be manually measured and entered, or an ADCP distance source can be used (VTG in this case). Right: Multiple transects are overlain, then averaged to improve the accuracy of the result (black dashed line) and exported as a .csv file.

Advantages of this approach:

- Bad transects can be filtered out (unchecked in QRev), or by comparison with other transects to remove outliers.
- Channel width can be manually entered if needed, or comes from the average projected width of the selected transects for the selected distance reference.
- Multiple transects are averaged, which increases the accuracy of output data.

See Biggs (2022) for detailed instructions how to use the software tool and apply this method.

Link for software: <https://github.com/HamishBiggs/DroneFlow>

Contact Hamish.Biggs@niwa.co.nz for any questions or custom data processing applications.

¹⁵ It is currently being developed in New Zealand and will be known as SouthPAN (Southern Positioning Augmentation Network) <https://www.linz.govt.nz/data/geodetic-services/satellite-based-augmentation-system>

Appendix B Cross sections from depth sounders with GPS

Bathymetry data collected with depth sounders and spatially referenced with RTK GPS or PPK GPS requires post processing to generate cross sections. Typically, these systems will be configured to either log continuously (i.e., with a uniform timestep between measurements), or the GPS system will trigger a measurement from the depth sounder when the system moves a defined distance. Tilt correction should be automatically performed by the depth sounder; however, the spatial location of the depth sounder (from GPS) will require correction and resampling to address: (1) path loops, (2) excess data near banks, (3) non-straight paths across the river, and (4) multiple passes. This correction involves projection of data onto a cross section defined by left bank and right bank points (Figure B-1), the resampling, interpolating, and smoothing data (Figure B-2).

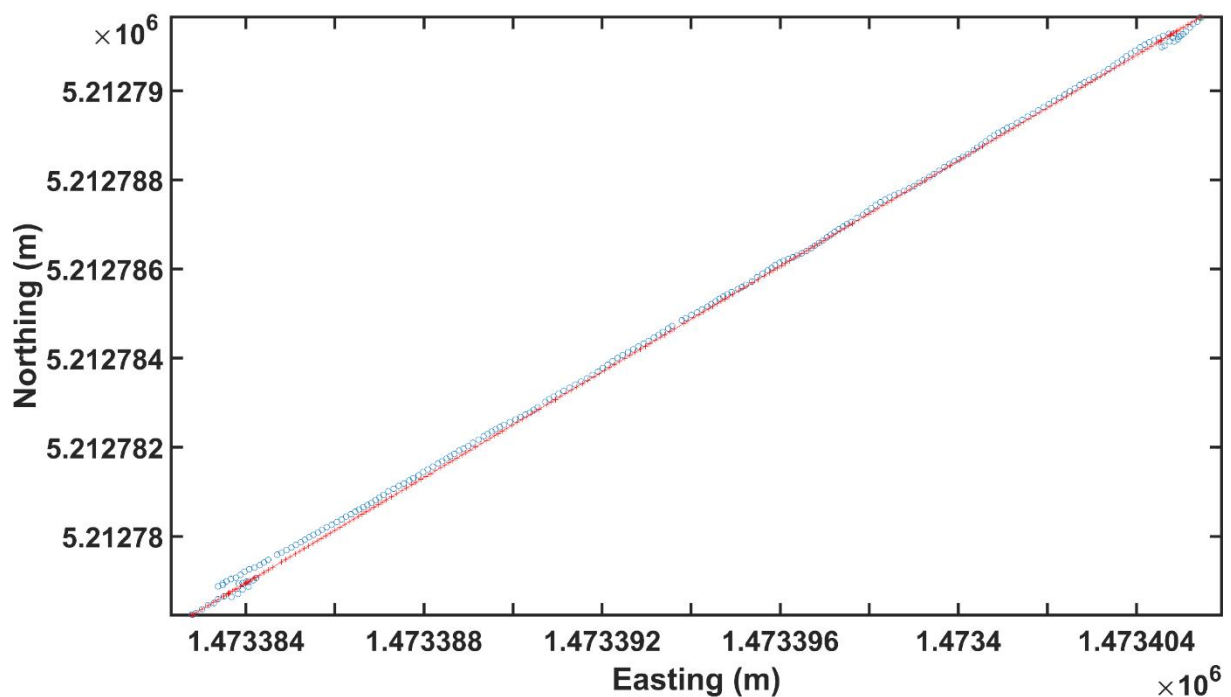


Figure B-1: Measurement locations from are projected onto the cross section unit vector.

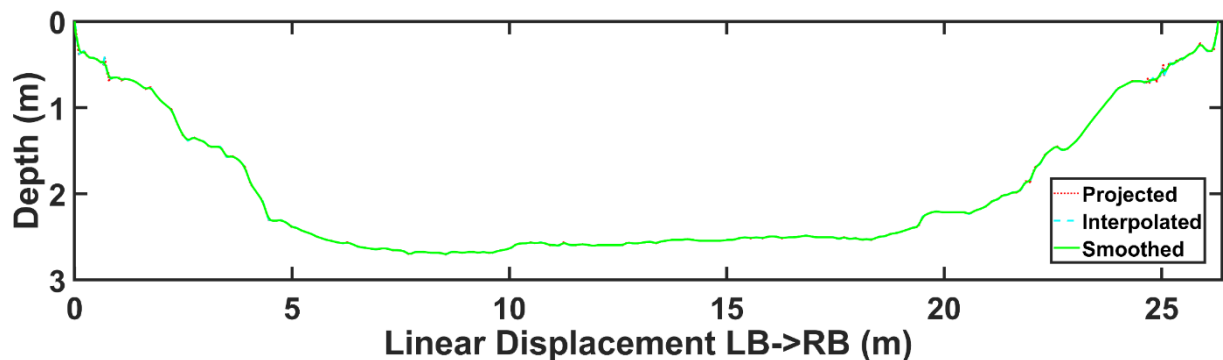


Figure B-2: The cross section and depth measurements are linearly interpolated and smoothed.

During the 'drone flow' project a Tritech PA500 depth sounder and a Trimble R10 RTK GPS Rover were used, with MATLAB code for processing data provided through the GitHub repository <https://github.com/HamishBiggs/DroneFlow> and the script 'CrossSectionsFromRTKGPSBathy.m'.

To use this code, the data processing steps are:

- Pre-process depth sounder data by adding the transducer depth.
- Pre-process near bank regions that were manually surveyed with the RTK GPS survey staff and rover, by subtracting bed elevation from water surface elevation to obtain depth.
- Create a new .csv file for all the depth and RTK GPS data, with the following columns and header {Name,Easting_m,Northing_m,CorrectedDepth_m}.
- Copy the depth sounder data and manual surveying data into the .csv file.
 - The first data record should correspond to 'Bank 1', while the last should correspond to 'Bank 2'. These define the cross section unit vector and cross section extent. Depth should be approximately zero here.
 - Manually find these bank points and rearrange the order if needed, then save the .csv file.
- Run 'CrossSectionsFromRTKGPSBathy.m'.

The provided MATLAB script then:

- Loads the data.
- Projects it onto the cross section unit vector (Figure B-1).
- Removes any data beyond the limits defined by the 'Bank 1' and 'Bank 2' locations.
- Takes user input as to which bank is the 'True Left'.
- Interpolates and smooths the depth data (Figure B-2).
- Exports the cross section data as .csv files of cross stream displacement (true left bank to true right bank) with separate files provided for 'Depth' and 'Elevation'.

These exported .csv files of cross section bathymetry can then be easily used for discharge calculations (i.e., surface image velocimetry) and other applications.

Please contact Hamish.Biggs@niwa.co.nz for further information, to obtain compiled executable versions of files if needed, or for help modifying these functions for different equipment and applications.